On the Theory of Risk-Aware Agents: Bridging Actor-Critic and Economics

Michal Nauman 12 Marek Cygan 13

Abstract

Risk-aware Reinforcement Learning (RL) algorithms like SAC and TD3 were shown empirically to outperform their risk-neutral counterparts in a variety of continuous-action tasks. However, the theoretical basis for the pessimistic objectives these algorithms employ remains unestablished, raising questions about the specific class of policies they are implementing. In this work, we apply the expected utility hypothesis, a fundamental concept in economics, to illustrate that both risk-neutral and risk-aware RL goals can be interpreted through expected utility maximization using an exponential utility function. This approach reveals that risk-aware policies effectively maximize value certainty equivalent, aligning them with conventional decision theory principles. Furthermore, we propose Dual Actor-Critic (DAC). DAC is a risk-aware, model-free algorithm that features two distinct actor networks: a pessimistic actor for temporal-difference learning and an optimistic actor for exploration. Our evaluations of DAC across various locomotion and manipulation tasks demonstrate improvements in sample efficiency and final performance. Remarkably, DAC, while requiring significantly less computational resources, matches the performance of leading model-based methods in the complex dog and humanoid domains.

1. Introduction

Deep Reinforcement Learning (RL) is still in its infancy, with a variety of tasks unsolved (Sutton & Barto, 2018; Hafner et al., 2023) or solved within an unsatisfactory amount of environment interactions (Zawalski et al., 2022; Schwarzer et al., 2023). Whereas increasing the Replay Ratio (RR) (ie. the number of parameter updates per envi-

Preprint, currently under peer review, Copyright 2024 by the authors.

ronment interactions step) is a promising general approach for increasing sample efficiency and final performance of RL agents (Janner et al., 2019; Chen et al., 2020; Nikishin et al., 2022), it is characterized by quickly diminishing gains (D'Oro et al., 2022) combined with linearly increasing computational cost (Rumelhart et al., 1986; Kingma & Ba, 2014). Moreover, the limitations of robot hardware and data acquisition frequency constrain the maximum achievable replay ratio (Smith et al., 2022). As such, it is worthwhile to pursue orthogonal techniques such as enhancing the properties of the underlying model-free agents. One continuously researched theme deals with finding risk attitudes that efficiently handle the *exploration-exploitation* dilemma (Ciosek et al., 2019; Moskovitz et al., 2021).

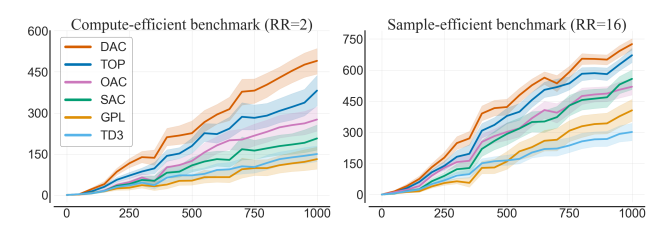


Figure 1. We assess the proposed method (DAC) on a range of DeepMind Control and MetaWorld tasks listed in Table 2. We compare DAC to a variety of model-free algorithms, in both low and high replay regimes. In high replay ratio, all algorithms are scaled by resetting. Our findings indicate that DAC achieves significant improvements in performance and sample efficiency compared to the Soft Actor-Critic. The Y-axis denotes the interquartile mean and the 95% confidence interval. 21 tasks, 1mln environment steps, and 10 seeds per task.

The attitudes towards risk of algorithmic agents have been researched in multiple contexts. For instance, a risk-seeking approach of optimism in the face of uncertainty has been identified as an effective exploration strategy, minimizing regret during the learning process (Wang et al., 2020b; Neu & Pike-Burke, 2020). Conversely, risk-averse, pessimistic learning strategies have proven beneficial in counteracting value overestimation caused by temporal difference errors (Hasselt, 2010; Fujimoto et al., 2018). However, there is a disconnect between these risk-aware strategies and the foundational theories of RL, particularly in how they relate to the goal of value maximization. As a result, despite the empirical success of risk-aware agents, the specific class of policies they implement remains ambiguous.

¹Informatics Institute, University of Warsaw ²Ideas National Centre for Research and Development ³Nomagic. Correspondence to: Michal Nauman <nauman.mic@gmail.com>.

In this paper, we study the reinforcement learning objective aligned with the principles of decision theory: the Von Neumann-Morgenstern theorem (Von Neumann & Morgenstern, 1947); and the expected utility hypothesis (Von Neumann & Morgenstern, 1947; Kahneman & Tversky, 1979). We show that, in contrast to pure value maximization, the proposed theory allows for derivation of both risk-neutral (e.g., DDPG (Silver et al., 2014)) and risk-aware approaches (e.g., TD3 (Fujimoto et al., 2018)). We demonstrate that the pessimistic updates in state of the art algorithms such as SAC (Haarnoja et al., 2018), REDQ (Chen et al., 2020), or TOP (Moskovitz et al., 2021) can be derived from expected utility maximization under an exponential utility function. Furthermore, we introduce Dual Actor-Critic (DAC), a risk-aware algorithm with two actors: optimistic and pessimistic. In DAC, each actor is trained independently using gradient backpropagation of a distinct objective: the optimistic actor aims to maximize an upper value bound for exploration, while the pessimistic actor focuses on a lower bound for temporaldifference (TD) targets (Fujimoto et al., 2018; Haarnoja et al., 2018). DAC also features an automatic adjustment mechanism to balance the divergence between these actors, allowing for adaptability to various tasks without hyperparameter tuning. We evaluate DAC on a diverse set of locomotion and manipulation tasks and find that, despite its simplicity, DAC achieves state of the art sample efficiency and performance. Below, we outline our contributions:

- 1. We introduce a generalized utility-based actor-critic objective, capable of formalizing both risk-neutral and risk-aware actor-critic algorithms. Based on the proposed theory, we demonstrate that the policies enacted by risk-aware algorithms align with the certainty equivalent of value, and as such are optimal in the decision theoretic context. We show that a policy optimizing Clipped Double Q-learning is approximately utility-optimal under an exponential utility.
- 2. We introduce Dual Actor-Critic (DAC), a risk-aware actor-critic framework featuring a dual actor network configuration. In DAC, each actor is trained through gradient backpropagation stemming from a specific objective that reflects different degrees of risk appetite. We establish the optimistic policy loss function and implement a system for online gradient-based adjustment of optimism hyperparameters. This feature enables DAC to effectively adapt to varying degrees of uncertainties, as well as different reward scales, without the need for manual hyperparameter tuning.
- 3. We show that DAC outperforms benchmarks in terms of both sample efficiency and final performance, in both low and high replay regimes. Notably, DAC solves the dog domain, reaching the performance of significantly more complex model-based methods. To facilitate further research, we perform ablations on various design and hyperparameter choices (over 5000 training runs). We release the implemen-

tation of DAC under the following URL.

2. Background

2.1. Reinforcement Learning

We consider an infinite-horizon Markov Decision Process (MDP) (Puterman, 2014) which is described with a tuple (S, A, r, p, γ) , where states S and actions A are continuous, $r_{s,a}$ is the transition reward, p(s) is the initial state distribution and $\gamma \in (0,1]$ is a discount factor. A policy $\pi(a|s)$ is a state-conditioned action distribution with entropy denoted as $\mathcal{H}(s)$. Soft Value is the sum of expected discounted return and state entropies from following the policy at a given state $V^{\pi}(s) = \mathbb{E}_{a \sim \pi} [r_{s,a} + \alpha \mathcal{H}(s) + \gamma V^{\pi}(s')]$, with α denoting the entropy temperature parameter. Q-value is the expected discounted return from performing an action and following the policy thereafter $Q^{\pi}(s, a) = [r_{s,a} + \gamma V^{\pi}(s')].$ A policy is said to be optimal if it maximizes the expected value of the possible starting states s_0 , such that $\dot{\pi} = \arg \max_{\pi \in \Pi} \mathcal{E}_{s_0 \sim p} V^{\pi}(s_0)$, with $\dot{\pi}$ denoting the optimal policy and Π denoting the considered set of policies (eg. Gaussian). In off-policy actor-critic, there is continuous gradient-based learning of both Q-values (critic) and the policy (actor). The critic parameters θ are updated by minimizing the variants of SARSA temporal-difference on transitions T = (s, a, r, s'), with T being sampled from past experiences (Fujimoto et al., 2018; Haarnoja et al., 2018):

$$\dot{\theta} = \arg\min_{\theta} \mathop{\mathbf{E}}_{T \sim \mathcal{D}} \left(Q_{\theta}(s, a) - r_{s, a} - \gamma V_{\theta}^{lb}(s') \right)^{2}$$
 (1)

Here, $Q_{\theta}(s,a)$ is the critic output, V_{θ}^{lb} is the bootstrap value derived from a target network, and \mathcal{D} is the experience buffer (Mnih et al., 2015). Under certain conditions $Q_{\theta}(s,a)$ is guaranteed to perfectly approximate the Q-value under the policy from which the bootstrap is sampled (Van Seijen et al., 2009; Sutton & Barto, 2018). The policy parameters ϕ are updated to seek locally optimal values approximated by the critic (Ciosek & Whiteson, 2020):

$$\dot{\pi}_{\phi} = \underset{\pi \in \Pi}{\arg \max} \underset{s \sim \mathcal{D}}{\mathbf{E}} V_{\theta}^{lb}(s) \tag{2}$$

In this equation, π_{ϕ} represents the actor, and V_{θ}^{lb} is the estimated lower-bound value, calculated using the critic:

$$V_{\theta}^{lb}(s) \approx Q_{\theta}^{lb}(s, a) - \alpha \log \pi_{\phi}(a|s), \quad a \sim \pi_{\phi}(s)$$
 (3)

Where Q_{θ}^{lb} represents the lower bound Q-value approximation, $\log \pi_{\phi}$ is the state-action entropy. Employing V_{θ}^{lb} , a

technique called Clipped Double Q-Learning (CDQL), has proven effective in mitigating value overestimation in Temporal Difference (TD) learning (Van Hasselt et al., 2016; Fujimoto et al., 2018). The lower bound is derived from a critic ensemble, often with two networks (Fujimoto et al., 2018; Haarnoja et al., 2018; Ciosek et al., 2019):

$$\begin{split} Q_{\theta}^{lb}(s,a) &= \min \left(Q_{\theta}^1(s,a), Q_{\theta}^2(s,a) \right) \\ &= \underbrace{\frac{1}{2} \left(Q_{\theta}^1(.) + Q_{\theta}^2(.) \right)}_{\text{Mean}} - \underbrace{\frac{1}{2} \left| Q_{\theta}^1(.) - Q_{\theta}^2(.) \right|}_{\text{Standard Deviation}} \quad \text{(4)} \end{split}$$

The observation led to a generalization of the lower bound (Moskovitz et al., 2021; Cetin & Celiktutan, 2023):

$$V_{\theta}^{\beta}(s) \triangleq V_{\theta}^{\mu}(s) + \beta V_{\theta}^{\sigma}(s)$$

$$Q_{\theta}^{\beta}(s, a) \triangleq Q_{\theta}^{\mu}(s, a) + \beta Q_{\theta}^{\sigma}(s, a)$$
(5)

In this formulation, β represents the degree of pessimism, and (μ,σ) denote the mean and standard deviation of the value model ensemble and $V_{\theta}^{\beta}(s) = \mathrm{E}_{a \sim \pi} Q_{\theta}^{\beta}(s,a) - \log \pi_{\phi}(a|s)$. In this formulation, the risk level of the lower bound is modulated by β . In case of $\beta = -1$, the pessimistic value Q_{θ}^{β} equals the CDQL lower bound Q_{θ}^{lb} . A non-zero β indicates a departure from risk-neutrality: positive β yields a pessimistic lower bound, while negative β results in an optimistic upper bound. Optimizing actor-critic modules towards a pessimistic lower bound discourages state actions with high critic ensemble disagreement, a phenomenon known as pessimistic underexploration (Ciosek et al., 2019; Cetin & Celiktutan, 2023). Given fixed policy parameters, it follows that optimization towards the risk-aware bootstrap leads value approximator V_{θ} to an output:

$$V_{\theta}(s) = \mathop{\mathbf{E}}_{a_i \sim \pi} \sum_{i=0}^{\infty} \gamma^i \left(r_{s_i, a_i} + \alpha \mathcal{H}(s_i) + \beta V_{\theta}^{\sigma}(s_i) \right)$$
 (6)

The subscript i denotes the outcomes in states following state s. Thus, for given ϕ the difference between the risk-aware value (resulting from bootstrapping with V_{θ}^{β}), and risk-neutral values (resulting from bootstrapping with V_{θ}^{μ} and denoted as \bar{V}_{θ}) is proportional to the expected values of the discounted sum of critic disagreements, as shown below:

$$V_{\theta}(s) - \bar{V}_{\theta}(s) = \mathop{\mathbf{E}}_{a_i \sim \pi} \beta \sum_{i=0}^{\infty} \gamma^i V_{\theta}^{\sigma}(s_i)$$
 (7)

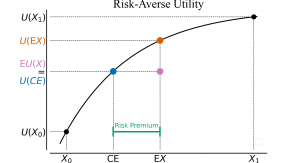
As such, if the difference is nonzero, the pessimistic policy diverges from the risk-neutral policy and yields regret. Despite this, numerous effective off-policy algorithms adopt a risk-aware objective, leaning towards either pessimism or optimism (Fujimoto et al., 2018; Haarnoja et al., 2018; Ciosek et al., 2019; Cetin & Celiktutan, 2023).

2.2. Expected Utility Theorem

The Von Neumann–Morgenstern Theorem (Von Neumann & Morgenstern, 1947) posits that an agent whose preferences adhere to four axioms (completeness, transitivity, continuity, and independence), has a utility function $\mathcal{U}(x)$ that function enables the comparison of the preferences. The expected utility hypothesis (Von Neumann & Morgenstern, 1947; Kahneman & Tversky, 1979) states that agents choose between risky options by comparing their expected utility, such that given $x^i \sim X^i$, it follows that $X^1 \succeq X^2 \iff \mathrm{E}\ U(x^1) \geq \mathrm{E}\ U(x^2)$. This implies optimization of utility, rather than its input (Stiglitz, 1997).

$$\dot{x} = \arg\max_{x} \mathop{\mathbf{E}}_{x^{i} \sim X} \mathcal{U}(x^{i}) \tag{8}$$

Due to non-linearity, there can be a discrepancy between $\arg\max E\ U(x^i)$ and $\arg\max E\ x^i$. Certainty Equivalent (CE) of X, denoted as X^c , measures the impact of uncertainty on utility-optimal choices: $\mathcal{U}(X^c)=E\ \mathcal{U}(X)$. CE presents a deterministic value offering the same utility as a random event and varies based on risk preference, which is influenced by the utility function. Risk-averse utilities yield a CE lower than the expected value, while risk-seeking leads to a higher CE. The exponential utility, $\mathcal{U}(x,\beta)=e^{\beta x}$, is a simple model for risk-awareness, with β determining the risk-appetite. We show the risk-aware utilities in Figure 2.



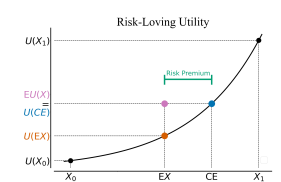


Figure 2. The risk appetite follows from the Jensen inequality: a convex utility indicates risk-seeking behavior, as evidenced by a CE exceeding EX; conversely, a concave utility signifies risk-aversion, reflected in a CE that is smaller than EX.

3. Theory of Risk-Aware Agents

In risk-aware methods, actor-critic modules are updated based on the risk-aware value V_{θ}^{β} . Consequently, the policy derived from this approach deviates from the optimal policy stemming from pure value maximization, as indicated by the regret defined in Equation 7. Notably, many state-of-the-art algorithms adopt non-risk-neutral strategies (Moskovitz et al., 2021; Hiraoka et al., 2021; D'Oro et al., 2022). However, the risk-aware correction, as outlined in Equation 7,

is not fully explicated by existing RL theory and does not emerge from pure value maximization problems. To this end, the efficacy of risk-aware agents is often attributed to two factors: risk-averse pessimism is justified by welldocumented value overestimation in temporal learning (Hasselt, 2010; Fujimoto et al., 2018; Kumar et al., 2020), while risk-loving optimism is supported by lower regret guarantees for exploration (Chen et al., 2017; Ciosek et al., 2019; Schrittwieser et al., 2020). In this section, we posit that both riskaware and risk-neutral algorithms can be formalized as optimizing an expected utility objective. We consider a cycle of policy evaluation and improvement steps (denoted with subscript t): $V_0 \to \pi_0 \to V_1^{\pi_0} \to \pi_1 \to \dots \to V_t^{\pi_{t-1}} \to \pi_t$. In this sequence, V^{π} continually approximates the on-policy value. We focus on an arbitrary time-step t, representing the policy and value at this step as $\pi = \pi_t$ and $V = V_t^{\pi_{t-1}}$ respectively. Thus, we analyze a single step of policy evaluation and improvement. The value approximations $V^{i}(s)$ are samples from the distribution V(s), which is assumed to have finite moments and expected value denoted by V^{μ} :

$$V^{\mu} \triangleq \underset{s \sim p}{\text{E}} \underset{i \sim \mathcal{V}}{\text{E}} V^{i}(s) = \text{E} V^{i}(s), \quad V^{i}(s) \sim \mathcal{V}(s) \quad (9)$$

Where p represents a desired probability measure, such as discounted stationary distribution. Assuming that the expected value of $V^i(s)$ is an unbiased estimator of the onpolicy value, the standard approach requires the policy to optimize for V^μ , such that $\pi = \arg\max_{\pi \in \Pi} V^\mu$. However, this is not the approach applied by the risk-aware algorithms. Given an invertible, increasing utility function \mathcal{U} , we define the *certainty equivalent value*, denoted as V^c :

$$V^{c} \triangleq \mathcal{I} \to \mathcal{U} V^{i}(s) = V^{\mu} + \Upsilon \tag{10}$$

Above, the inverted utility function is denoted by $\mathcal{I}=\mathcal{U}^{-1}$ and Υ denotes the value risk premium stemming from the utility. In this context, the certainty equivalent value represents the deterministic amount that amortizes the uncertainties associated with the value stochasticity. Building on the expected utility objective from Equation 8, we define the *certainty equivalence policy* that seeks to maximize the expected utility of values:

Lemma 3.1. For any monotonically increasing Von Neumann–Morgenstern utility:

$$\pi_c = \operatorname*{arg\,max}_{\pi \in \Pi} \to \mathcal{U} \ V^i(s) = \operatorname*{arg\,max}_{\pi \in \Pi} V^c$$
 (11)

The lemma stems directly from the monotonicity of the utility function. Above, π_c represents the policy that optimizes for the expected utility of values, which we term

the *certainty equivalent policy*. As follows, the certainty equivalent policy is greedy with respect to the certainty equivalent value and aligns with the expected utility hypothesis, wherein the agent seeks to maximize the expected utility of returns. This outcome contrasts with achieving the maximal value possible, as is typically sought in standard RL objectives. The certainty equivalent policy π_c optimizes for values that are not generally equal to the risk-neutral values. Therefore, we establish that the utility-based objective generalizes the RL objective, identifying conditions under which π_c and π are equivalent.

Lemma 3.2. For any linearly increasing utility function:

$$\Upsilon = 0 \quad \wedge \quad V^c = V^\mu \quad \wedge \quad \pi_c = \pi \tag{12}$$

This implies that given linear utility, the certainty equivalence objective converges with the traditional RL objective, making the certainty equivalent policies identical to the policy optimizing the risk-neutral objective. This is the case because a linear utility implies risk-neutrality. Hence, risk-neutral algorithms like DDPG can be interpreted as linear utility agents optimizing the certainty equivalent objective. We also explore scenarios where the utility is non-linear and thus diverges from the traditional RL objective.

Lemma 3.3. Assume \mathcal{U} is invertible, infinitely differentiable and its Taylor expansion is convergent. Denote $\mathcal{U}^n(V^\mu)$ as the nth derivative of \mathcal{U} calculated at V^μ then:

$$\Upsilon \approx \mathcal{I} \to \sum_{n=1}^{\infty} \frac{\mathcal{U}^n(V^{\mu})}{n!} (V^i(s) - V^{\mu})^n$$
 (13)

The lemma is an application of the Taylor series to the utility, calculated at point V^{μ} . It shows that the discrepancy between the certainty equivalent value and the risk-neutral value depends on moments of $\mathcal{V}(s)$. We now show that the risk-aware value V^{β} stems from an exponential utility.

Theorem 3.4. Denote expected value $V^{\mu} = \mathbb{E}_{s \sim p} V^{\mu}(s)$, exponential utility $\mathcal{U}(V^i, \beta) = e^{2\beta V^i(s)}$, then the certainty equivalent $V^c = \mathbb{E}_{s \sim p} V^c(s)$ is approximately equal to the pessimistic value $V^{\beta} = \mathbb{E}_{s \sim p} V^{\beta}(s)$:

$$V^{c}(s) \approx V^{\mu}(s) + \beta \mathop{\rm E}_{i \sim \mathcal{V}} \left(V^{i}(s) - V^{\mu}(s) \right)^{2}$$

$$\approx V^{\beta}(s) \tag{14}$$

Consequently, risk-aware agents like TD3 or SAC can be understood as optimizing for the utility-based objective, pursuing certainty equivalent rather than the maximal possible

values. Interestingly, the utility-based objective introduces a pessimistic correction proportional to the variance of approximation models, slightly diverging from the CDQL that uses the standard deviation. Exploring alternative utility functions and their impact on risk attitudes, as well as approximation via further order Taylor polynomial presents a promising direction for research in risk-aware RL. All calculations are detailed in Appendix A.

4. Dual Actor-Critic

Dual Actor-Critic (DAC) is a risk-aware, off-policy algorithm that addresses the exploration and temporal-difference (TD) learning dichotomy in actor-critic algorithms. Usually, actor-critic algorithms use a single actor for both exploration (sampling actions for new transitions) and TD learning (calculating TD targets), which requires balancing between optimism for exploration (Wang et al., 2020b) and pessimism for avoiding value overestimation (Hasselt, 2010). DAC resolves this by employing optimistic and pessimistic actors, with each actor being updated to optimize the certainty equivalent value stemming from utilities with unique risk appetites. The optimistic actor is trained to maximize the upper Q-value bound and is solely used for exploration, while the pessimistic actor, guided by the lower Q-value bound, is used for TD learning and evaluation. This separation allows DAC to explore efficiently without the risk of value overestimation. DAC also addresses the shortcomings of Optimistic Actor-Critic (OAC) (Ciosek et al., 2019). By relaxing the first-order Taylor approximation and explicitly modeling the optimistic policy via a neural network DAC can approximate the maximum of arbitrary complexity upper bound (Hornik et al., 1989). DAC adjusts the optimism levels associated with the upper bound such that the two policies reach a predefined divergence target. As such, DAC alleviates the tandem problem induced by off-policy learning using two actors. The DAC algorithm follows the policy iteration framework in which the policy evaluation and policy improvement steps are interleaved and performed on dataset of previous experiences. DAC is structured around two components: a critic ensemble of k models (following the standard SAC/TD3 implementation we use k = 2 models) and the dual actor comprising pessimistic and optimistic actors denoted π^p_ϕ and π^o_η respectively. Each actor is associated with an exponential utility function $\mathcal{U}(x,\beta)$ with different levels of risk appetite, denoted as β^p and β^o for the pessimistic and optimistic actors. The critic Q_{θ} is bootstrapped via the pessimistic certainty equivalent value:

$$\dot{\theta}_i = \underset{\theta}{\operatorname{arg\,min}} \underset{T \sim \mathcal{D}}{\operatorname{E}} \left(Q_{\theta}(s, a) - r_{s, a} - \gamma V_{\theta}^{\beta^p}(s') \right)^2 \quad (15)$$

Where $V_{\theta}^{\beta^p}(s')$ is the certainty equivalent bootstrap under

- 1: **Input:** π^p_ϕ pessimistic actor; π^o_η optimistic actor; Q^π_θ critic; α temperature; β^o optimism; τ KL weight;
- 2: **Hyperparameters:** β^p pessimism; \mathcal{KL}^* target KL;
- 3: Sample action from the optimistic actor s', r = ENV.STEP(a) $a \sim \pi_n^o$
- 4: Add transition to the replay buffer BUFFER.ADD(s, a, r, s')
- 5: **for** i = 1 **to** ReplayRatio **do**
- Sample batch of transitions $s, a, r, s' \sim \text{BUFFER.SAMPLE}$
- Update critic using pessimistic actor (Eq. 15) $\theta \leftarrow \nabla_{\theta} (Q_{\theta}^{\pi} r \gamma (Q_{\beta^{p}}^{\pi} \alpha \log \pi_{\phi}))^{2} \quad a' \sim \pi_{\phi}^{p}$ Update pessimistic actor (Eq. 17) 7:
- $\phi \leftarrow \nabla_{\phi}(\alpha \log \pi_{\phi} Q_{\beta^p}^{\pi}) \quad a \sim \pi_{\phi}^p$
- Update optimistic actor (Eq. 18) 9: $\eta \leftarrow \nabla_{\eta} (\tau KL(\pi^p_{\phi} | \pi^o_{\eta}) - Q^{\pi}_{\beta^o}) \quad a \sim \pi^o_{\eta}$
- Update entropy temperature 10: $\alpha \leftarrow \nabla_{\alpha} \alpha (\mathcal{H}^* - \mathcal{H}(s))$
- Update optimism (Eq. 20) 11:
- $\beta^{o} \leftarrow \nabla_{\beta^{o}}(\beta^{o} \beta^{p})(\frac{1}{|A|}KL(\pi^{p}_{\phi}|\pi^{o}_{\eta}) \mathcal{KL}^{*})$ $Update \ KL \ weight \ (Eq. \ 20)$ $\tau \leftarrow \nabla_{\tau}\tau(\frac{1}{|A|}KL(\pi^{p}_{\phi}|\pi^{o}_{\eta}) \mathcal{KL}^{*})$ 12:
- $\begin{array}{l} \textit{Update target network} \\ Q_t^{\pi} = \text{Polyak}(Q_{\theta}^{\pi}, Q_t^{\pi}) \end{array}$ 13:
- 14: end for

Figure 3. Pseudo-code shows DAC training step, where changes with respect to SAC are colored. We summarize the most important aspects of the proposed approach: *Dual Actors* - the pessimistic actor optimizes lower bound value (line 8) and is used for TD learning (line 7), the optimistic actor optimizes a regularized upper bound (line 9) and is used for exploration (line 3); Online Tuning - the optimism of upper bound (β^{o}) and the KL weight (τ) is adjusted such that the divergence target is met (lines 11 and 12).

the pessimistic utility, stemming from the critic model Q_{θ} .

$$V_{\theta}^{\beta^p}(s) \approx Q_{\theta}^{\beta^p}(s, a) - \log \pi_{\phi}(a|s), \quad a \sim \pi_{\phi}^p(s)$$
 (16)

With $Q_{\theta}^{\beta^p}(s,a) = Q_{\theta}^{\mu}(s,a) + \beta^p Q_{\theta}^{\sigma}(s,a)$. Subtracting the maximum entropy term $\log \pi_{\phi}(a|s)$ from the pessimistic value ensures consistency between the soft values pursued by the pessimistic actor and the soft values approximated by the critic. The pessimistic actor is updated to maximize the certainty equivalent values under its utility:

$$\dot{\pi}_{\phi}^{p} = \underset{\pi \in \Pi}{\arg \max} \, \mathbf{E} \, e^{\, 2\beta^{p} V_{\theta}^{i}(s)} \approx \underset{\pi \in \Pi}{\arg \max} \, \underset{s \sim \mathcal{D}}{\mathbf{E}} V_{\theta}^{\beta^{p}}(s) \quad (17)$$

As shown in Theorem 3.4, optimizing for the expected utility objective leads to a risk-aware value, ensuring convergence to the optimal policy under CDQL assumptions (Fujimoto et al., 2018). This setup aligns the objectives of the critic and the pessimistic actor in DAC with the pessimistic SAC. The optimistic actor π_{η}^{o} , is defined by an objective function that maximizes a utility expression that accounts for the divergence between the two actors:

$$\dot{\pi}_{\eta}^{o} = \underset{\pi \in \Pi}{\arg \max} \operatorname{E} e^{2\beta^{p}(V_{\theta}^{i}(s) - \tau KL(\bar{\pi}_{\phi}^{p}(s)|\pi_{\eta}^{o}(s)))} \\
\approx \underset{\pi \in \Pi}{\arg \max} \underset{s \sim \mathcal{D}}{\operatorname{E}} V_{\theta}^{\beta^{o}}(s) - \tau KL(\bar{\pi}_{\phi}^{p}(s)|\pi_{\eta}^{o}(s)) \tag{18}$$

Above, $V_{\theta}^{\beta^o}(s)$ is the value certainty equivalent stemming from optimistic utility, KL represents the Kullback-Leibler divergence between the two actors, and τ is the penalty weight for this divergence. Incorporating two actors that are used for TD and exploration respectively, it is natural to assign distinct entropy levels to each policy. Our approach involves computing the KL divergence between the pessimistic policy π_{ϕ}^p and a modified optimistic policy, denoted as $\bar{\pi}_{\eta}^o$. This modified policy is characterized by a standard deviation that is m-times smaller than that of the optimistic policy π_{η}^o , with $m \in (0, \infty)$. We refer to m as exploration variance multiplier. Detailed methodology for this KL divergence calculation is provided in Appendix C and Equation 44. We calculate the optimistic value $V_{\theta}^{\beta^o}(s)$ according to:

$$V_{\theta}^{\beta^{o}}(s) \approx Q_{\theta}^{\mu}(s, a) + \beta^{o}Q_{\theta}^{\sigma}(s, a), \quad a \sim \pi_{\phi}^{o}$$
 (19)

As such, both risk-aware values are approximated via the critic evaluated at actions sampled from the respective actor. The goal of KL regularization used by the optimistic actor is to achieve divergence small enough to ensure good coverage of the pessimistic policy in exploration data, yet large enough to maintain the optimistic policy's exploration effectiveness. In practice, the level of KL divergence is influenced by three factors: the KL penalty weight τ , the difference in risk appetites between the actors $(\beta^o - \beta^p)$, and the critic ensemble disagreement $Q^{\sigma}_{\theta}(s, a)$, which varies based on reward scale, environmental uncertainty, and network architecture. To achieve a balanced divergence between the two actors, we allow gradient-based adjustments in τ and $(\beta^o - \beta^p)$, while assuming a fixed β^p . The optimization objectives for τ and β^o are thus formulated to adapt to varying conditions, ensuring efficient exploration and exploitation balance in the DAC framework in different environments:

$$\dot{\beta}^{o} = \underset{\beta^{o}}{\operatorname{arg\,min}} (\beta^{o} - \beta^{p}) \underset{s \sim \mathcal{D}}{\operatorname{E}} \Delta^{D}(s), \ \beta^{o} \in (\beta^{p}, \infty)
\dot{\tau} = \underset{\tau}{\operatorname{arg\,min}} \ \tau \underset{s \sim \mathcal{D}}{\operatorname{E}} \Delta^{D}(s), \ \tau \in (0, \infty)$$
(20)

Table 1. We evaluate the performance impact of omitting certain DAC components. We detail the setting in Sections 5 and E. 15 tasks, 500k steps, 10 seeds per task.

DAC DESIGN	RR=2	RR=16
SINGLE POLICY π^o_η	0.42	0.68
DETERMINISTIC π^p_ϕ	0.62	0.82
DETERMINISTIC π^o_η	0.84	0.77
DAC SIMPLIFIED	1.01	0.88
No KL REGULARIZATION	0.64	0.82
No $ au$ and eta Adjustment	0.91	0.92
No β Adjustment	0.96	0.89
No $ au$ Adjustment	0.91	0.92
DAC REGULAR	1.00	1.00

Where $\Delta^D(s)$ represents the discrepancy between the recorded and target KL divergence:

$$\Delta^{D}(s) = \frac{1}{|A|} KL(\pi_{\phi}^{p}(s)|\pi_{\eta}^{o}(s)) - \mathcal{KL}^{*}$$
 (21)

The mechanism adjusts β^o and τ based on the comparison between the empirical and target KL divergences. When the empirical divergence exceeds the target, β^o decreases to a limit of β^p , and τ increases. Conversely, a smaller empirical divergence than the target leads to an increase in β^o and a decrease in τ . This dual adjustment allows DAC to regulate the divergence between two policy actors, maintaining control even when β^o reaches its lower bound. We depict the different levels of optimism achieved in various tasks in Figure 10. For policy modeling, we utilize the Tanh-transformed Gaussian distribution, $\mathcal{T}(\mu, \sigma)$ (Haarnoja et al., 2018; Wang et al., 2020a). We implement the optimistic actor in two architectures: simplified (denoted with subscript s) and regular (denoted with subscript r). In the simplified architecture, the network directly models the optimistic policy's distribution parameters for a given state as $f_s(\eta, s) = (\mu_n^o(s), \sigma_n^o(s)),$ defining the optimistic policy as $\pi_{\eta}^{o}(s) = \mathcal{T}(\mu_{\eta}^{o}(s), \sigma_{\eta}^{o}(s))$. The regular architecture introduces a perturbation to the pessimistic policy parameters:

$$f_r(\eta, s) = (\bar{\mu}_{\eta}^o(s), \bar{\sigma}_{\eta}^o(s)) \pi_{\eta}^o = \mathcal{T}((\mu_{\rho}^p(s) + \bar{\mu}_{\eta}^o(s)), (\sigma_{\rho}^p(s) * \bar{\sigma}_{\eta}^o(s)))$$
 (22)

Unlike the simplified configuration, the regular architecture of DAC offers a significant advantage in terms of managing the KL divergence between the pessimistic and optimistic actors. The regular DAC defines the optimistic actor's output as a perturbation of the pessimistic policy. This choice

anchors the two actors together, and to minimize divergence, the optimistic actor needs to adjust its output independently of any modifications to the pessimistic policy (ie. independent of the pessimistic policy location, the optimistic actor has to adjust its output towards 0). Such mechanism ensures a stable and controlled divergence between the two actors, as shown in Figure 10. Further details on design and implementation, as well as a derivation of DAC for a non-soft value function are shared in Appendix C.

5. Experiments

Our experimental framework is based on the JaxRL code base (Kostrikov, 2021). We assess the performance of DAC across a diverse set of locomotion and manipulation tasks, sourced from the DeepMind Control (DMC) (Tassa et al., 2018) and single-task MetaWorld (MW) (Yu et al., 2020) suites. This includes hard environments such as dog and assembly. To ensure comparability between the two suites and achieve a single performance metric, we multiply the MW success rates by 1000. DAC is benchmarked against an array of both risk-neutral and risk-aware baselines, including TD3 (Fujimoto et al., 2018), SAC (Haarnoja et al., 2018), OAC (Ciosek et al., 2019), TOP (Moskovitz et al., 2021), and GPL (Cetin & Celiktutan, 2023). In high replay ratio scenarios we implement scaling-by-resetting on all algorithms, as outlined in (D'Oro et al., 2022). Furthermore, DAC performance is evaluated against other notable algorithms such as MPO (Abdolmaleki et al., 2018), D4PG (Barth-Maron et al., 2018), REDQ (Chen et al., 2020), DreamerV3 (Hafner et al., 2023), and TD-MPC (Hansen et al., 2022). Evaluation metrics are calculated via the RLiable package (Agarwal et al., 2021). Details regarding the experimental setup and hyperparameters are available in Appendices E and F.

Low and High Replay Regimes We align our experiments with the state-of-the-art SAC implementation, standardizing the common hyperparameters across all algorithms (D'Oro et al., 2022). We employ uniform network architectures and ensemble of two critics, as advocated in previous work (Fujimoto et al., 2018; Haarnoja et al., 2018; Ciosek et al., 2019; Moskovitz et al., 2021; Cetin & Celiktutan, 2023). We consider 21 locomotion and manipulation tasks, ranging from medium to hard difficulty, detailed in Table 2. Each task is run for 1mln environment steps. We investigate two replay regimes: a compute-efficient regime, involving 2 gradient updates per environment step, and a sample-efficient regime, using 16 gradient updates per step. The latter also includes full-parameter resets every 160kenvironment steps, in line with the approach proposed by D'Oro et al. (2022). Other experimental details are discussed in Appendix E. Our results, illustrated in Figures and 1, 4 and 6 show that DAC surpasses the benchmark performance in both replay regimes. This performance gap

is particularly notable in the low replay setup, underscoring DAC efficacy in compute-sensitive applications. A key observation depicted in Figure 4, is DAC ability to match the performance of scaled by resetting SAC (SR-SAC) despite employing substantially less resources: DAC matches the final performance of SR-SAC with 8-times smaller replay; and SR-DAC matches the final SR-SAC performance with almost 2-times fewer environment steps. Notably, we observe this efficiency improvement across both DMC and MW suites while using the same set of hyperparameters.

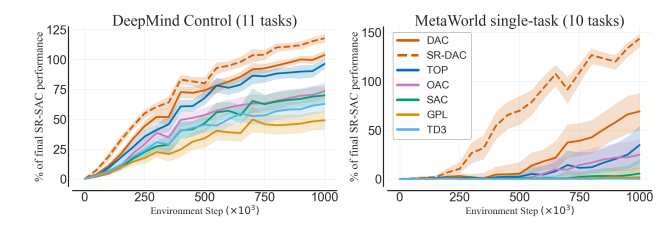


Figure 4. Low replay DAC matches the performance of SR-SAC (scaled by resetting SAC) despite using 8-times less gradient steps. SR-DAC reaches SR-SAC final performance (1mln steps) in 500k environment step, yielding 2-times better sample efficiency. The Y-axis denotes the % of the final SR-SAC performance with the 95% CI. 21 tasks, 1mln steps and 10 seeds per task.

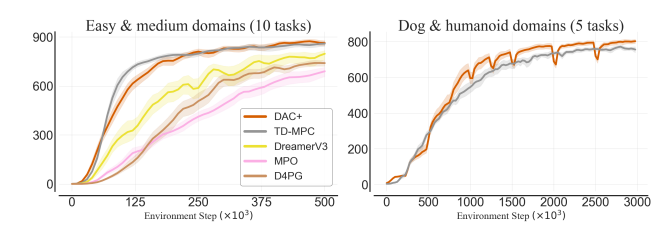


Figure 5. Our results indicate that, despite reduced complexity and lower wall-clock time requirements, DAC achieves comparable performance to model-based algorithms. Easy and medium difficulty tasks use 10 seeds, dog and humanoid tasks use 5 seeds.

Comparison Against Model-Based RL We assess the performance of DAC against established model-based methods, focusing on 15 tasks from DMC benchmark detailed in Table 3. This includes 10 tasks of easy to medium difficulty from the DreamerV3 benchmark (Hafner et al., 2023), run for 500k steps, as well as 5 more challenging tasks (three from the dog domain and two from the humanoid domain), each run for 3mln steps. The dog domain is particularly notable for its complexity, with few methods achieving significant performance (Hansen et al., 2022; Xu et al., 2023). TD-MPC, a recent model-based approach, has been documented to achieve effective policies in both dog and humanoid domains (Hansen et al., 2022). This approach employs more complex model architectures with a greater number of parameters compared to model-free algorithms. To partially offset this disparity, we modified DAC critic to mimic the critic used in TD-MPC, by adding a single

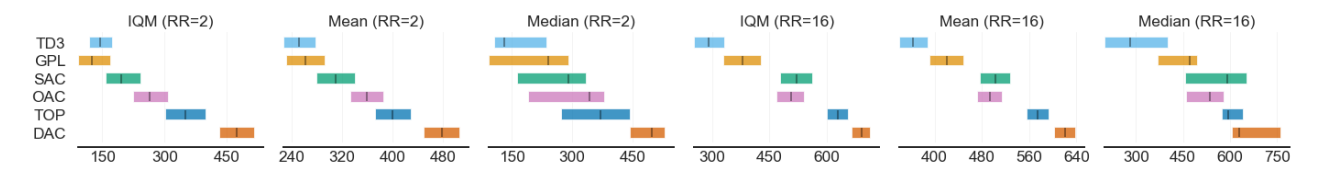


Figure 6. DAC achieves statistically significant improvement in both low and high replay regimes. We ensure comparability between DMC and MW suites by scaling the MW success rates by 1000. In high replay regime, all algorithms use scaling by resetting with resets performed every 160k steps. Final performance in 1mln steps training, 21 tasks listed in Table 2, with 10 random seeds per task.

hidden layer and layer normalization (Ball et al., 2023), resulting in a variant named DAC+. As presented in Figure 5, DAC+ achieves competitive performance in the dog domain, marginally surpassing TD-MPC. Notably, DAC achieves this performance despite being a model-free algorithm.

Design and Hyperparameter Sensitivity We explore how DAC performance is influenced by variations in hyperparameters and design. We conduct evaluations across 15 tasks from DMC and MW, detailed in Table 4, and consider both replay ratios. This analysis encompasses over 5k training runs, the results of which are shown in Figure 7 and Table 1. In terms of hyperparameters, our findings indicate stable performance across all tested hyperparameter values, with all low and high replay configurations of DAC surpassing SAC and SR-SAC respectively. In the design choice experiment, we evaluate the performance impact of various changes to DAC, including variations such as deterministic policies. We discuss these results in Appendix E.

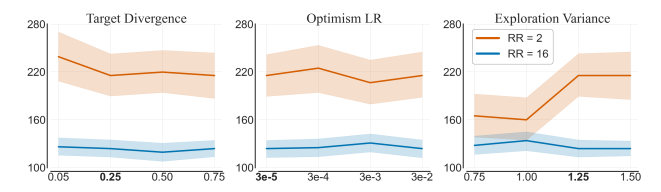


Figure 7. We evaluate 4 values for each hyperparameter (X-axis). The bold values correspond to the setting used in other experiments. Y-axis measures the performance of DAC and SR-DAC as % of SAC and SR-SAC respectively. 15 tasks, 500k steps and 10 seeds.

Additional Experiments In Appendix D, we detail supplementary experiments conducted to further evaluate DAC. In particular, we study the effects of the simplified and regular architectures of DAC, as discussed in Section 4. Interestingly, we find that the simplified architecture underperforms only on the most complex considered environments. These results are presented in Figures 11 and Table 1. Another area of focus is the implementation of layer normalization within DAC. This regularization technique was shown to improve the performance of RL agents on a variety tasks (Hiraoka et al., 2021; Li et al., 2022; Lyle et al., 2023). We find that using layer norm further improves DAC performance on locomotion tasks, and detail the results in Figure 12. Finally,

we test if the dual architecture indeed mitigates the overestimation associated with an optimistic TD update. As shown in Figure 13, DAC does not induce value overestimation.

6. Limitations

Main limitation of DAC is its dual-actor network framework, which incurs slightly higher memory and computation costs relative to the standard SAC. In our implementation, DAC wall-clock time is around 15% longer than SAC/TD3. Furthermore, DAC poses a higher degree of off-policy learning than SAC or TD3. While we have found DAC to be robust with respect to the tandem problem, there might exist tasks in which maintaining the divergence is more complex.

7. Conclusions

In this work, we apply the expected utility theorem to reason about the empirical effectiveness of risk-aware actor-critic algorithms. In particular, we demonstrate that policies derived from the commonly used pessimistic objective are approximately utility-optimal when aligned with an exponential utility function. We think that the proposed framework is interesting as it revisits the foundational decision-theoretic perspective of RL — namely, optimization within the utility space rather than the space of utility inputs. Consequently, we propose that this conceptual link between empirically successful actor-critic methods and decision theory could potentially offer insights into the risk preferences observed in human behavior.

Furthermore, we present DAC, a risk-aware actor-critic framework. DAC employs two actors with distinct risk appetites to optimize their respective expected utility functions. The pessimistic actor focuses on TD learning and evaluation, while the optimistic actor facilitates exploration. We evaluate DAC on various locomotion and manipulation tasks and compare it with over ten baseline algorithms. We find that DAC demonstrates significant performance improvements relative to other model-free methods and is competitive with leading model-based approaches. Finally, we investigate DAC performance robustness across diverse hyperparameter configurations and find that the experiments affirm its practical applicability.

IMPACT STATEMENT

In this paper, we analyze the pessimistic RL algorithms through the expected utility theorem and introduce a sample-efficient RL algorithm inspired by microeconomic principles. This approach to integrating behavioral theories into RL presents significant opportunities to improve agents. However, it also introduces a reverse application: using RL insights to inform microeconomic understanding and human behavior. This latter brings important ethical considerations.

Applying economic theories to RL can enhance machine decision-making to more closely resemble human judgment. However, the consequences of machines operating in roles traditionally occupied by humans must be carefully analyzed. Similarly, applying RL principles to microeconomics offers perspectives on human decision-making and economic models, but should be done cautiously to avoid oversimplifying the human behavior and societal interactions.

ACKNOWLEDGMENTS

We would like to thank Łukasz Kuciński for his help in developing the ideas presented in this paper. We also thank Piotr Miłoś and Gracjan Góral for their valuable help and discussions. Marek Cygan is co-financed by the National Centre for Research and Development as a part of the EU-supported Smart Growth Operational Programme 2014-2020 (POIR.01.01.01-00-0392/17-00). The experiments were performed using the Entropy cluster funded by NVIDIA, Intel, the Polish National Science Center grant UMO-2017/26/E/ST6/00622, and the ERC Starting Grant TOTAL. We also gratefully acknowledge Polish high-performance computing infrastructure PLGrid (HPC Center: ACK Cyfronet AGH) for providing computer facilities and support within computational grant no. PLG/2023/016783

References

- Abdolmaleki, A., Springenberg, J. T., Tassa, Y., Munos, R., Heess, N., and Riedmiller, M. Maximum a posteriori policy optimisation. In *International Conference on Learning Representations*, 2018.
- Agarwal, R., Schwarzer, M., Castro, P. S., Courville, A. C., and Bellemare, M. Deep reinforcement learning at the edge of the statistical precipice. *Advances in neural information processing systems*, 34:29304–29320, 2021.
- Amari, S.-I. Natural gradient works efficiently in learning. *Neural computation*, 10(2):251–276, 1998.
- Auer, P., Cesa-Bianchi, N., and Fischer, P. Finite-time analysis of the multiarmed bandit problem. *Machine learning*, 47:235–256, 2002.

- Ba, J. L., Kiros, J. R., and Hinton, G. E. Layer normalization. *arXiv preprint arXiv:1607.06450*, 2016.
- Ball, P., Parker-Holder, J., Pacchiano, A., Choromanski, K., and Roberts, S. Ready policy one: World building through active learning. In *International Conference on Machine Learning*, pp. 591–601. PMLR, 2020.
- Ball, P. J., Smith, L., Kostrikov, I., and Levine, S. Efficient online reinforcement learning with offline data. 2023.
- Barth-Maron, G., Hoffman, M. W., Budden, D., Dabney, W., Horgan, D., Dhruva, T., Muldal, A., Heess, N., and Lillicrap, T. Distributed distributional deterministic policy gradients. In *International Conference on Learning Representations*, 2018.
- Cetin, E. and Celiktutan, O. Learning pessimism for reinforcement learning. In *Proceedings of the AAAI Conference on Artificial Intelligence*, volume 37, pp. 6971–6979, 2023.
- Chen, R. Y., Sidor, S., Abbeel, P., and Schulman, J. Ucb exploration via q-ensembles. *arXiv preprint arXiv:1706.01502*, 2017.
- Chen, X., Wang, C., Zhou, Z., and Ross, K. W. Randomized ensembled double q-learning: Learning fast without a model. In *International Conference on Learning Representations*, 2020.
- Ciosek, K. and Whiteson, S. Expected policy gradients for reinforcement learning. *Journal of Machine Learning Research*, 21(2020), 2020.
- Ciosek, K., Vuong, Q., Loftin, R., and Hofmann, K. Better exploration with optimistic actor critic. *Advances in Neural Information Processing Systems*, 32, 2019.
- D'Oro, P., Schwarzer, M., Nikishin, E., Bacon, P.-L., Bellemare, M. G., and Courville, A. Sample-efficient reinforcement learning by breaking the replay ratio barrier. In *The Eleventh International Conference on Learning Representations*, 2022.
- Filippi, S., Cappé, O., and Garivier, A. Optimism in reinforcement learning and kullback-leibler divergence. In 2010 48th Annual Allerton Conference on Communication, Control, and Computing (Allerton), pp. 115–122. IEEE, 2010.
- Foster, D. J., Krishnamurthy, A., Simchi-Levi, D., and Xu, Y. Offline reinforcement learning: Fundamental barriers for value function approximation. In *Conference on Learning Theory*, pp. 3489–3489. PMLR, 2022.
- Fujimoto, S., Hoof, H., and Meger, D. Addressing function approximation error in actor-critic methods. In *International conference on machine learning*, pp. 1587–1596. PMLR, 2018.

- Garivier, A. and Moulines, E. On upper-confidence bound policies for switching bandit problems. In *International Conference on Algorithmic Learning Theory*, pp. 174–188. Springer, 2011.
- Gogianu, F., Berariu, T., Rosca, M. C., Clopath, C., Busoniu, L., and Pascanu, R. Spectral normalisation for deep reinforcement learning: an optimisation perspective. In *International Conference on Machine Learning*, pp. 3734– 3744. PMLR, 2021.
- Haarnoja, T., Zhou, A., Hartikainen, K., Tucker, G., Ha, S., Tan, J., Kumar, V., Zhu, H., Gupta, A., Abbeel, P., et al. Soft actor-critic algorithms and applications. arXiv preprint arXiv:1812.05905, 2018.
- Hafner, D., Pasukonis, J., Ba, J., and Lillicrap, T. Mastering diverse domains through world models. arXiv preprint arXiv:2301.04104, 2023.
- Han, X., Chen, X., and Liu, L.-P. Gan ensemble for anomaly detection. In *Proceedings of the AAAI Conference on Artificial Intelligence*, volume 35, pp. 4090–4097, 2021.
- Hansen, N., Wang, X., and Su, H. Temporal difference learning for model predictive control. In *International Conference on Machine Learning*, PMLR, 2022.
- Hasselt, H. Double q-learning. *Advances in neural information processing systems*, 23, 2010.
- Hiraoka, T., Imagawa, T., Hashimoto, T., Onishi, T., and Tsuruoka, Y. Dropout q-functions for doubly efficient reinforcement learning. In *International Conference on Learning Representations*, 2021.
- Hornik, K., Stinchcombe, M., and White, H. Multilayer feedforward networks are universal approximators. *Neural networks*, 2(5):359–366, 1989.
- Janner, M., Fu, J., Zhang, M., and Levine, S. When to trust your model: Model-based policy optimization. *Advances* in Neural Information Processing Systems, 32, 2019.
- Kahneman, D. and Tversky, A. Prospect theory: An analysis of decision under risk. *Econometrica*, 47(2):263–292, 1979.
- Kakade, S. M. A natural policy gradient. Advances in neural information processing systems, 14, 2001.
- Kaufmann, E., Cappé, O., and Garivier, A. On bayesian upper confidence bounds for bandit problems. In *Artificial* intelligence and statistics, pp. 592–600. PMLR, 2012.
- Kingma, D. P. and Ba, J. Adam: A method for stochastic optimization. *arXiv preprint arXiv:1412.6980*, 2014.

- Kostrikov, I. JAXRL: Implementations of Reinforcement Learning algorithms in JAX, 10 2021. URL https://github.com/ikostrikov/jaxrl.
- Krogh, A. and Hertz, J. A simple weight decay can improve generalization. Advances in neural information processing systems, 4, 1991.
- Kumar, A., Gupta, A., and Levine, S. Discor: Corrective feedback in reinforcement learning via distribution correction. *Advances in Neural Information Processing Systems*, 33:18560–18572, 2020.
- Kuznetsov, A., Shvechikov, P., Grishin, A., and Vetrov, D. Controlling overestimation bias with truncated mixture of continuous distributional quantile critics. In *International Conference on Machine Learning*, pp. 5556–5566. PMLR, 2020.
- Laskin, M., Lee, K., Stooke, A., Pinto, L., Abbeel, P., and Srinivas, A. Reinforcement learning with augmented data. *Advances in neural information processing systems*, 33: 19884–19895, 2020.
- Lee, K., Laskin, M., Srinivas, A., and Abbeel, P. Sunrise: A simple unified framework for ensemble learning in deep reinforcement learning. In *International Conference on Machine Learning*, pp. 6131–6141. PMLR, 2021.
- Li, Q., Kumar, A., Kostrikov, I., and Levine, S. Efficient deep reinforcement learning requires regulating overfitting. In *The Eleventh International Conference on Learning Representations*, 2022.
- Liu, Z., Li, X., Kang, B., and Darrell, T. Regularization matters in policy optimization-an empirical study on continuous control. In *International Conference on Learning Representations*, 2020.
- Lyle, C., Zheng, Z., Nikishin, E., Pires, B. A., Pascanu, R., and Dabney, W. Understanding plasticity in neural networks. *arXiv preprint arXiv:2303.01486*, 2023.
- Mnih, V., Kavukcuoglu, K., Silver, D., Rusu, A. A., Veness, J., Bellemare, M. G., Graves, A., Riedmiller, M., Fidjeland, A. K., Ostrovski, G., et al. Human-level control through deep reinforcement learning. *nature*, 518(7540): 529–533, 2015.
- Moskovitz, T., Parker-Holder, J., Pacchiano, A., Arbel, M., and Jordan, M. Tactical optimism and pessimism for deep reinforcement learning. *Advances in Neural Information Processing Systems*, 34:12849–12863, 2021.
- Neu, G. and Pike-Burke, C. A unifying view of optimism in episodic reinforcement learning. *Advances in Neural Information Processing Systems*, 33:1392–1403, 2020.

- Nikishin, E., Schwarzer, M., D'Oro, P., Bacon, P.-L., and Courville, A. The primacy bias in deep reinforcement learning. In *International conference on machine learn*ing, pp. 16828–16847. PMLR, 2022.
- Osband, I., Blundell, C., Pritzel, A., and Van Roy, B. Deep exploration via bootstrapped dqn. *Advances in neural information processing systems*, 29, 2016.
- Osband, I., Aslanides, J., and Cassirer, A. Randomized prior functions for deep reinforcement learning. *Advances in Neural Information Processing Systems*, 31, 2018.
- Pathak, D., Gandhi, D., and Gupta, A. Self-supervised exploration via disagreement. In *International conference on machine learning*, pp. 5062–5071. PMLR, 2019.
- Peters, J. and Schaal, S. Natural actor-critic. *Neurocomputing*, 71(7-9):1180–1190, 2008.
- Protter, M. H., Charles Jr, B., et al. *A first course in real analysis*. Springer Science & Business Media, 2012.
- Puterman, M. L. Markov decision processes: discrete stochastic dynamic programming. John Wiley & Sons, 2014.
- Rumelhart, D. E., Hinton, G. E., and Williams, R. J. Learning representations by back-propagating errors. *nature*, 323(6088):533–536, 1986.
- Schäfer, L., Christianos, F., Hanna, J. P., and Albrecht, S. V. Decoupled reinforcement learning to stabilise intrinsically-motivated exploration. In *Proceedings of* the 21st International Conference on Autonomous Agents and Multiagent Systems, pp. 1146–1154, 2022.
- Schrittwieser, J., Antonoglou, I., Hubert, T., Simonyan, K., Sifre, L., Schmitt, S., Guez, A., Lockhart, E., Hassabis, D., Graepel, T., et al. Mastering atari, go, chess and shogi by planning with a learned model. *Nature*, 588(7839): 604–609, 2020.
- Schulman, J., Levine, S., Abbeel, P., Jordan, M., and Moritz, P. Trust region policy optimization. In *International* conference on machine learning, pp. 1889–1897. PMLR, 2015.
- Schwarzer, M., Ceron, J. S. O., Courville, A., Bellemare, M. G., Agarwal, R., and Castro, P. S. Bigger, better, faster: Human-level atari with human-level efficiency. In *International Conference on Machine Learning*, pp. 30365–30380. PMLR, 2023.
- Sekar, R., Rybkin, O., Daniilidis, K., Abbeel, P., Hafner, D., and Pathak, D. Planning to explore via self-supervised world models. In *International Conference on Machine Learning*, pp. 8583–8592. PMLR, 2020.

- Seyde, T., Gilitschenski, I., Schwarting, W., Stellato, B., Riedmiller, M., Wulfmeier, M., and Rus, D. Is bangbang control all you need? solving continuous control with bernoulli policies. *Advances in Neural Information Processing Systems*, 34:27209–27221, 2021.
- Seyde, T., Schwarting, W., Karaman, S., and Rus, D. Learning to plan optimistically: Uncertainty-guided deep exploration via latent model ensembles. In *Conference on Robot Learning*, pp. 1156–1167. PMLR, 2022.
- Silver, D., Lever, G., Heess, N., Degris, T., Wierstra, D., and Riedmiller, M. Deterministic policy gradient algorithms. In *International conference on machine learning*, pp. 387–395. PMLR, 2014.
- Silver, D., Schrittwieser, J., Simonyan, K., Antonoglou, I., Huang, A., Guez, A., Hubert, T., Baker, L., Lai, M., Bolton, A., et al. Mastering the game of go without human knowledge. *nature*, 550(7676):354–359, 2017.
- Smith, L., Kostrikov, I., and Levine, S. A walk in the park: Learning to walk in 20 minutes with model-free reinforcement learning. *arXiv preprint arXiv:2208.07860*, 2022.
- Srivastava, N., Hinton, G., Krizhevsky, A., Sutskever, I., and Salakhutdinov, R. Dropout: a simple way to prevent neural networks from overfitting. *The journal of machine learning research*, 15(1):1929–1958, 2014.
- Stiglitz, J. E. *Microeconomics*. New York, NY: WW Norton, 1997.
- Sutton, R. S. and Barto, A. G. *Reinforcement learning: An introduction*. MIT press, 2018.
- Tassa, Y., Doron, Y., Muldal, A., Erez, T., Li, Y., Casas, D. d. L., Budden, D., Abdolmaleki, A., Merel, J., Lefrancq, A., et al. Deepmind control suite. arXiv preprint arXiv:1801.00690, 2018.
- Van Hasselt, H., Guez, A., and Silver, D. Deep reinforcement learning with double q-learning. In *Proceedings of the AAAI conference on artificial intelligence*, volume 30, 2016.
- Van Seijen, H., Van Hasselt, H., Whiteson, S., and Wiering, M. A theoretical and empirical analysis of expected sarsa. In 2009 ieee symposium on adaptive dynamic programming and reinforcement learning, pp. 177–184. IEEE, 2009.
- Von Neumann, J. and Morgenstern, O. Theory of games and economic behavior, 2nd rev. 1947.

- Wang, C., Wu, Y., Vuong, Q., and Ross, K. Striving for simplicity and performance in off-policy drl: Output normalization and non-uniform sampling. In *International Conference on Machine Learning*, pp. 10070–10080. PMLR, 2020a.
- Wang, Y., Wang, R., Du, S. S., and Krishnamurthy, A. Optimism in reinforcement learning with generalized linear function approximation. In *International Conference on Learning Representations*, 2020b.
- Xie, T., Foster, D. J., Bai, Y., Jiang, N., and Kakade, S. M. The role of coverage in online reinforcement learning. In *The Eleventh International Conference on Learning Representations*, 2022.
- Xu, G., Zheng, R., Liang, Y., Wang, X., Yuan, Z., Ji, T., Luo, Y., Liu, X., Yuan, J., Hua, P., et al. Drm: Mastering visual reinforcement learning through dormant ratio minimization. arXiv preprint arXiv:2310.19668, 2023.
- Yahaya, S. W., Lotfi, A., and Mahmud, M. A consensus novelty detection ensemble approach for anomaly detection in activities of daily living. *Applied Soft Computing*, 83:105613, 2019.
- Yu, T., Quillen, D., He, Z., Julian, R., Hausman, K., Finn, C., and Levine, S. Meta-world: A benchmark and evaluation for multi-task and meta reinforcement learning. In *Conference on robot learning*, pp. 1094–1100. PMLR, 2020.
- Zawalski, M., Tyrolski, M., Czechowski, K., Odrzygozdz, T., Stachura, D., Piekos, P., Wu, Y., Kucinski, L., and Milos, P. Fast and precise: Adjusting planning horizon with adaptive subgoal search. In *The Eleventh International* Conference on Learning Representations, 2022.
- Zhan, W., Huang, B., Huang, A., Jiang, N., and Lee, J. Offline reinforcement learning with realizability and single-policy concentrability. In *Conference on Learning Theory*, pp. 2730–2775. PMLR, 2022.

LIST OF FIGURES AND TABLES

- Figure 1 aggregate sample efficiency in low and high replay regimes.
- Figure 2 basic model of risk-averse and risk-loving utility.
- Figure 3 pseudo-code of DAC learning step.
- Figure 4 SR-SAC relative performance in low and high replay regimes.
- Figure 5 DAC as compared to model-based algorithms.
- Figure 6 final performance in low and high replay regimes.
- Figure 7 hyperparameter sensitivity experiments.
- Figure 8 tanh-normal distribution and MaxEnt RL.
- Figure 9 optimistic and pessimistic exploration.
- Figures 10 DAC adjustment mechanism in low and high replay regimes.
- Figure 11 simplified and regular DAC architectures in low and high replay regimes.
- Figure 12 investigation of layer normalization applied to DAC.
- Figure 13 dual architecture overestimation tests.
- Figures 14 task-specific results for the low and high replay experiments.
- Figures 15 and 16 task-specific results for the comparison against model-based algorithms.
- Table 1 results of the design choice experiments.
- Table 2 list of tasks used in the low and high replay experiments.
- Table 3 list of tasks used in the comparison against model-based experiments.
- Table 4 list of tasks used in the hyperparameter sensitivity and design choice experiments.

APPENDIX CONTENTS

- Derivations Appendix A
- Related Work Appendix B
- Further Description of DAC Appendix C
- Additional Experiments Appendix D
- Experimental Settings Appendix E
- Learning Curves and Hyperparameters Appendix F

A. Derivations

A.1. Theory of Risk-Aware Agents

We consider a single step of policy evaluation and improvement. We assume the value approximations $V^i(s)$ to be derived from a distribution $\mathcal{V}(s)$. This distribution is characterized by finite moments and an expected value V^{μ} :

$$V^{\mu} \triangleq \mathop{\mathbf{E}}_{s \sim p} \mathop{\mathbf{E}}_{i \sim \mathcal{V}} V^{i}(s) = \mathop{\mathbf{E}} V^{i}(s), \quad V^{i}(s) \sim \mathcal{V}(s)$$
(23)

Here, p denotes a specific probability measure of interest, such as the discounted stationary distribution.

A.1.1. LEMMA 3.1

The problem of maximizing expected utility is formulated as follows:

$$\pi_c = \operatorname*{arg\,max}_{\pi \in \Pi} \to \mathcal{U} V^i(s) = \operatorname*{arg\,max}_{\pi \in \Pi} \mathcal{U} V^c(s) = \operatorname*{arg\,max}_{\pi \in \Pi} V^c(s)$$
(24)

Given that Von Neumann-Morgenstern utilities are monotonous, and in our assumption, increasing, the utility function can be omitted in this context.

A.1.2. LEMMA 3.2

If the utility function is linear, then:

$$\pi_c = \operatorname*{arg\,max}_{\pi \in \Pi} \to \mathcal{U} V^i(s) = \operatorname*{arg\,max}_{\pi \in \Pi} \mathcal{U} \to V^i(s) = \operatorname*{arg\,max}_{\pi \in \Pi} V^{\mu}(s)$$
(25)

Thus, it must be that $V^c(s) = V^{\mu}(s)$, which further implies $\Upsilon = 0$ and $\pi_c = \pi$.

A.1.3. LEMMA 3.3

With an invertible utility function \mathcal{U} , the certainty equivalent value, represented as V^c , is defined by:

$$V^c \triangleq \mathcal{I} \to \mathcal{U} V^i(s) \tag{26}$$

Here, $\mathcal{I} = \mathcal{U}^{-1}$ denotes the inverse of the utility function. Our goal is to approximate V^c using its Taylor series expansion around the point V^{μ} :

$$V^{c} \approx \mathcal{I} \to \sum_{n=0}^{\infty} \frac{\mathcal{U}^{n}(V^{\mu})}{n!} (V^{i}(s) - V^{\mu})^{n} \approx \mathcal{I} \to \left(\mathcal{U}(V^{\mu})(V^{i}(s) - V^{\mu})^{0} + \sum_{n=1}^{\infty} \frac{\mathcal{U}^{n}(V^{\mu})}{n!} (V^{i}(s) - V^{\mu})^{n} \right)$$

$$\approx V^{\mu} + \mathcal{I} \to \sum_{n=1}^{\infty} \frac{\mathcal{U}^{n}(V^{\mu})}{n!} (V^{i}(s) - V^{\mu})^{n}$$
(27)

Considering that $V^c = V^{\mu} + \Upsilon$, it follows that:

$$\Upsilon = \mathcal{I} \to \sum_{n=1}^{\infty} \frac{\mathcal{U}^n(V^{\mu})}{n!} (V^i(s) - V^{\mu})^n$$
(28)

Which demonstrates that the value risk premium is approximately equivalent to the higher order terms in the Taylor series expansion.

A.1.4. THEOREM 3.4

The exponential utility function is defined as:

$$\mathcal{U}(V^i) = e^{2\beta V^i} \tag{29}$$

Deviation of observations from expected values, addressing both state-sampling and model-sampling risks, is defined as:

$$u(s) \triangleq V^{\mu}(s) - V^{\mu}$$

$$\epsilon^{i}(s) \triangleq V^{i}(s) - V^{\mu}(s)$$
(30)

By definition, both deviations have an expected value of zero. The risk premium, reflecting its dependency on states, is defined as:

$$V^{c} = \mathop{\mathbb{E}}_{s \sim p} V^{\mu}(s) + \Upsilon(s) = V^{\mu} + \Upsilon \tag{31}$$

The pessimistic value is defined as:

$$V^{\beta} = \mathop{\mathbb{E}}_{s \sim p} V^{\mu}(s) + \beta V^{\sigma}(s) = V^{\mu} + \beta V^{\sigma}$$
(32)

Thus, the pessimistic value is equal to the certainty equivalent value if, for a given utility function, it is true that $\Upsilon(s) = \beta V^{\sigma}(s)$. We start the derivation by applying the exponential utility to the certainty equivalent value definition:

$$e^{2\beta V^{c}} = \underset{s \sim p}{\text{E}} \underset{i \sim \mathcal{V}}{\text{E}} e^{2\beta V^{i}(s)} = \underset{s \sim p}{\text{E}} \underset{i \sim \mathcal{V}}{\text{E}} e^{2\beta (V^{\mu}(s) + \epsilon^{i}(s))} = \underset{s \sim p}{\text{E}} \underset{i \sim \mathcal{V}}{\text{E}} e^{2\beta V^{\mu}(s)} e^{2\beta \epsilon^{i}(s))$$

$$= \underset{s \sim p}{\text{E}} e^{2\beta V^{\mu}(s)} \underset{i \sim \mathcal{V}}{\text{E}} e^{2\beta \epsilon^{i}(s))} = e^{2\beta V^{\mu}} \underset{s \sim p}{\text{E}} e^{2\beta u(s)} \underset{i \sim \mathcal{V}}{\text{E}} e^{2\beta \epsilon^{i}(s))$$
(33)

Inverting the utility function on the left-hand side (LHS) leads to:

$$V^{c} = V^{\mu} + \frac{1}{2\beta} \ln \mathop{\mathbf{E}}_{s \sim p} e^{2\beta u(s)} + \frac{1}{2\beta} \ln \mathop{\mathbf{E}}_{s \sim p} \mathop{\mathbf{E}}_{i \sim \mathcal{V}} e^{2\beta \epsilon^{i}(s)}$$
(34)

This implies that the value risk premium Υ is equal to:

$$\Upsilon = \underbrace{\frac{1}{2\beta} \ln \mathop{\mathbf{E}}_{s \sim p} e^{2\beta u(s)}}_{\text{State risk premium}} + \underbrace{\frac{1}{2\beta} \ln \mathop{\mathbf{E}}_{s \sim p} \mathop{\mathbf{E}}_{i \sim \mathcal{V}} e^{2\beta \epsilon^{i}(s)}}_{\text{Model risk premium}}$$
(35)

As such, the value risk premium is composed from terms stemming from each risk. Those terms can be approximated. We start by approximating the model risk premium, which we denote by $\Upsilon_{\mathcal{V}}$:

$$\Upsilon_{\mathcal{V}} = \frac{1}{2\beta} \ln \mathop{\mathbb{E}}_{s \sim p} \mathop{\mathbb{E}}_{i \sim \mathcal{V}} e^{2\beta \epsilon^{i}(s)}$$
(36)

Given that $\epsilon^i(s)$, by definition, centers around zero, we use the Maclaurin series which is convergent in the considered case:

$$\Upsilon_{\mathcal{V}} \approx \frac{1}{2\beta} \ln \mathop{\mathbf{E}}_{s \sim p} \mathop{\mathbf{E}}_{i \sim \mathcal{V}} \left(1 + 2\beta \epsilon^{i}(s) + 2\beta^{2} \epsilon^{i}(s)^{2} \right)$$
 (37)

Considering the second order of this polynomial and the fact that the first order is zero in expectation:

$$\Upsilon_{\mathcal{V}} \approx \frac{1}{2\beta} \ln \mathop{\mathbf{E}}_{s \sim p} \mathop{\mathbf{E}}_{i \sim \mathcal{V}} \left(1 + 2\beta^2 \epsilon^i(s)^2 \right)$$
(38)

Here, $\epsilon^i(s)^2$ represents the variance of the model distribution at state s. Thus, for optimization purposes, the approximate equality $\nabla V^c \approx \nabla V^\beta$ is practically established. To approximate the values, not just their gradients, the logarithm is approximated with a first-order Maclaurin series:

$$\Upsilon_{\mathcal{V}} \approx \frac{1}{2\beta} \mathop{\mathbf{E}}_{s \sim p} \mathop{\mathbf{E}}_{i \sim \mathcal{V}} 2\beta^2 \epsilon^i(s)^2 = \beta \mathop{\mathbf{E}}_{s \sim p} \mathop{\mathbf{E}}_{i \sim \mathcal{V}} (V^i(s) - V^\mu)^2$$
(39)

Thus, the pessimistic correction arises from the second-order Maclaurin approximation of the model risk's value risk premium. To finalize the proof, we demonstrate that the state risk premium Υ_s is approximately zero, using the first-order Maclaurin series:

$$\Upsilon_s = \frac{1}{2\beta} \ln \mathop{\mathbf{E}}_{s \sim p} e^{2\beta u(s)} \approx \frac{1}{2\beta} \ln \mathop{\mathbf{E}}_{s \sim p} \left(1 + 2\beta u(s) \right) = \frac{\ln 1}{2\beta} = 0 \tag{40}$$

Consequently, the final approximation for $\Upsilon(s)$ is:

$$\Upsilon(s) \approx \beta \mathop{\rm E}_{i \sim \mathcal{V}} (V^i(s) - V^\mu(s))^2 \tag{41}$$

Which concludes the derivation.

Proof summary The proof begins by defining deviations within the probability distributions used in the expectation operator. By definition, these deviations have an expected value of zero. Utilizing the characteristics of the exponential function, we separate the risk premiums associated with each distribution. We then apply the Maclaurin approximation to the utility function, observing that the first order approximation of the risk premium is zero, with only higher order terms impacting the calculations. In particular, the second order approximation equates to the variance of the distribution in question. When approximating the utility shift caused by state deviations, the first order approximation effectively nullifies their influence on the optimization process. In contrast, applying the second order approximation to the model deviations yields the variance in relation to the deviation of model output. This approach demonstrates how different order of approximations can distinctly affect the evaluation resulting objective, with first order approximation to a risk-aware utility retrieving a risk-neutral objective.

Additional comment We note that the approach outlined in this Section can be adapted to address uncertainties inherent to a range of RL problems. An interesting example is the estimation of values through single evaluations of the critic. In such scenarios, adopting a risk-loving utility function can lead to objectives resembling Maximum Entropy (MaxEnt) principles. This suggests a potential avenue for integrating other risk preferences into actor-critic like setting. Moreover, the proof for the result, as detailed, can be considerably streamlined when focusing on gradients with respect to value functions in the context of policy optimization. Specifically, the approximation of the logarithm can be abandoned when the interest lies in optimizing policies rather than the values themselves. Finally, the utility-based objective offers a foundation for developing various risk-aware algorithms. In particular, exploring different utility functions or higher-order approximations of these functions naturally leads to different certainty equivalent value objectives.

B. Related Work

B.1. Uncertainty Exploration and KL Constrained Policies

The exploration-exploitation dilemma has been the subject of extensive research. One prominent principle that has emerged in addressing this dilemma is Optimism in the Face of Uncertainty (OFU) (Auer et al., 2002; Filippi et al., 2010; Ciosek et al., 2019), which prioritizes actions with a balance of high expected rewards and uncertainty. Whereas OFU has been extensively studied in the tabular and bandit RL setting (Auer et al., 2002; Garivier & Moulines, 2011; Kaufmann et al., 2012), it has not yet become as standard in deep RL. However, it has been shown that DQN ensembles used for uncertainty-driven updates can provide performance improvements (Osband et al., 2016; Chen et al., 2017; Osband et al., 2018; Lee et al., 2021). Similarly, OAC (Ciosek et al., 2019) and TOP (Moskovitz et al., 2021) leverage uncertainty estimates over the state-action value function for exploration, albeit still using only pessimistic actor. On that note, (Schäfer et al., 2022) propose to use two actors, with one actor using some form of novelty exploration objective.

The optimism-driven exploration was also considered for model-based agents. Sekar et al. (2020) and Seyde et al. (2022) consider exploration driven by reward model ensemble. Similarly to DAC, Seyde et al. (2022) considers using an optimistic upper bound exploration policy and a distinct exploitation policy. Furthermore, agents like RP1 (Ball et al., 2020) leverage reward uncertainty despite access to the nominal rewards. Finally, a variety of agents that leverage MCTS have been proposed (Silver et al., 2017; Schrittwieser et al., 2020; Zawalski et al., 2022). On a different note, DAC might seem similar to natural actor-critic (Amari, 1998; Kakade, 2001; Peters & Schaal, 2008; Schulman et al., 2015) due to the KL constraint

in actor optimization. Whereas the natural policy gradient uses KL to enforce the similarity between policies resulting in subsequent updates, DAC leverages KL to constrain the optimistic policy to be within some range from the pessimistic policy that is used for TD learning. This allows for optimistic exploration without Q-value overestimation.

B.2. Comparison to OAC

DAC leverages two policies: a pessimistic one used for sampling the temporal-difference target and evaluation; and an optimistic one used for sampling transitions added to the experience buffer. Similarly to DAC, OAC performs evaluation and Bellman backups according to a pessimistic lower bound policy. However, DAC differs from OAC on three main design choices: how to model the optimistic policy; how to constraint the optimistic policy; and how to set the level of optimism β^{o} . Firstly, OAC models the optimistic policy by combining pessimistic policy with the linear approximation of Q-value upper bound, and as such uses one actor network. The linear approximation combined with constrained optimization results in simplistic solutions along the constraint boundary (Protter et al., 2012). As such, OAC's applicability is limited to small δ values due to the Taylor theorem. In contrast to that, DAC uses two actors. Modeling the second policy via an actor network allows for exploration policies that are far more complex than a linear approximator. Whereas this introduces a computational cost, employing techniques like delayed policy updates can result in costs smaller than that of OAC. Furthermore, OAC enforces a hard KL constraint by directly solving a Lagrangian. Since the O-value upper bound is approximated via a linear function, the solution is placed on the constraint boundary unless the slope is zero (Protter et al., 2012). In contrast, DAC imposes KL as a soft constraint. Paired with the neural network approximator, this allows DAC to balance the KL with potential gains to the upper bound and generate complex exploration policies. Finally, OAC treats β^o as a hyperparameter which is fixed during the training. Since values of Q^μ_π and Q^σ_π depend on reward scales, as well as aleatoric and epistemic uncertainty of the environment, the value of β^o has to be searched per task. Furthermore, due to decreasing critic disagreement as the training progresses, fixed levels of β^o yield decreasing the impact of uncertainty on the optimistic policy. DAC leverages that the desired level of optimism can be defined through divergence between the pessimistic baseline policy and the optimistic policy optimizing objective related to β^o . Such definition allows for dynamics adjustment of both β^o and the KL penalty weight τ .

C. Further Description of DAC

C.1. Pessimistic Actor

The pessimistic actor, denoted as π_{ϕ}^{p} , employs a soft policy target for optimization, as outlined in Equation 17. This actor operates entirely off-policy, utilizing data exclusively from the optimistic actor. The soft policy approach not only promotes state-dependent exploration (Haarnoja et al., 2018) but also helps in maintaining the hyperbolic tangent (Tanh) output in a non-saturated state (Wang et al., 2020a). Moreover, the pessimistic actor's inherent non-zero variance contributes to stabilizing the TD learning for the critic. While separating exploration and exploitation theoretically allows for zero variance in TD target sampling, our empirical evidence suggests that introducing noise regularizes the critic (see Table 1).

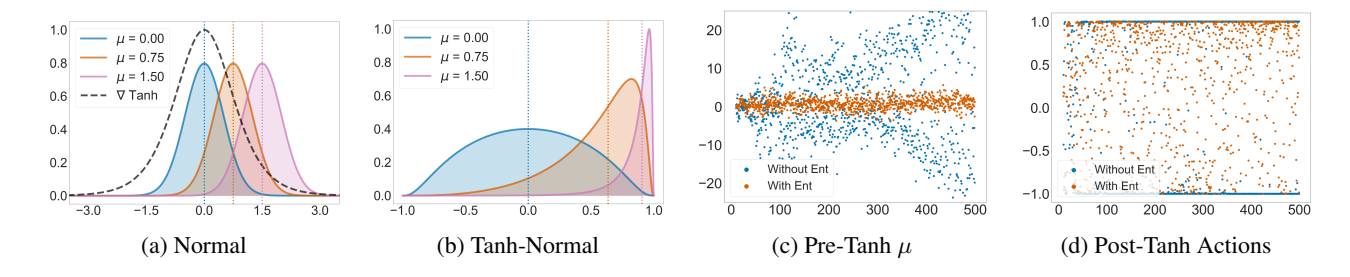


Figure 8. Soft policy learning prevents policy saturation. Figures 8a and 8b show three Gaussians and the Tanh transformed counterparts. Before Tanh transformation, all policies have equal variance (8a). However, since Tanh is nonlinear, applying the transformation changes the policy variance depending on the location of the mean (8b). Because of this effect, when using soft policy learning, the agent incurs loss when moving along the saturated portions of the Tanh activation function. Figures 8c and 8d show policy means and executed actions for SAC with and without soft policy learning on a Humanoid-Stand task. As follows, SAC without the entropy objectives follows a bang-bang policy, whereas regular SAC anchors the policy within the non-saturated portion of Tanh. To this end, soft policy learning reduces the risk of a bang-bang policy.

In the context of representing a policy with a Tanh-Normal distribution, soft policy learning serves two critical functions: promoting entropy and preventing saturation. Firstly, soft policy learning guarantees a certain degree of policy entropy, essential for exploration during the learning process (Haarnoja et al., 2018). This approach contrasts with methods like TD3 or TOP, where constant entropy is maintained across various states. By optimizing an objective function that balances entropy maximization with Q-values, our policy exhibits variable entropy depending on the state, encouraging exploration particularly in states with lower Q-values. Furthermore, the Tanh function's inherent saturation characteristic impacts the exploration. The further the unsquashed distribution's mean is from zero, the more the variance reduces post-squashing, as depicted in Figures 8a and 8b. Implementing soft policy learning thus incurs a loss when the policy deviates from zero. Figures 8c and 8d illustrate how this approach results in policies predominantly residing within the non-saturated Tanh region (Wang et al., 2020a), effectively avoiding extreme bang-bang policies (Seyde et al., 2021).

C.2. Optimistic Actor

The optimistic actor π_{η}^{o} , follows the optimistic certainty equivalence objective, detailed in Equation 18. This objective prioritizes the upper bound of Q-values, fostering a policy that embraces uncertainty and encourages actions leading to critic disagreement. Such a policy approach is known to generate more diverse samples and consequently, ensures better coverage of the state-action space (Pathak et al., 2019; Lee et al., 2021). This is significant as ensemble disagreement is often a surrogate for sample novelty (Yahaya et al., 2019; Han et al., 2021). Although traditional RL does not explicitly focus on coverage, recent research highlights the critical role of data diversity in RL (Xie et al., 2022; Foster et al., 2022; Zhan et al., 2022).

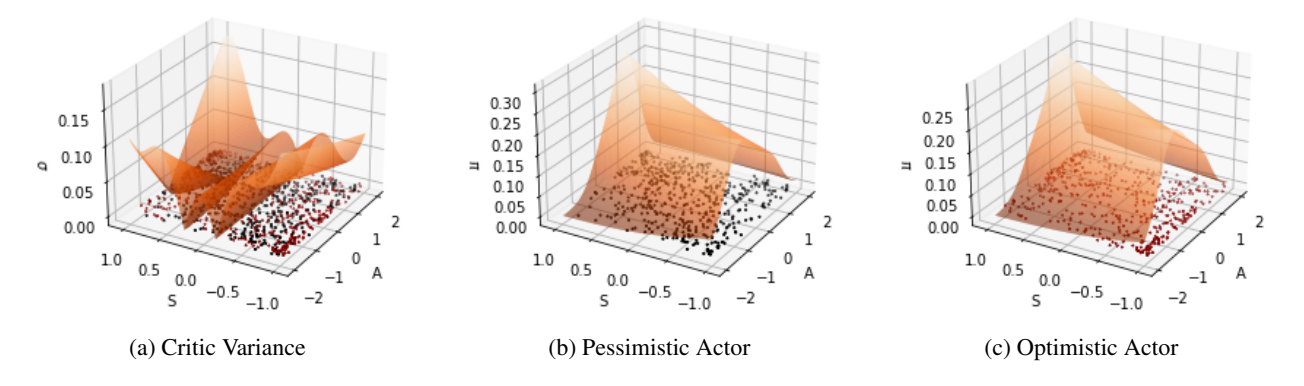


Figure 9. Pessimistic underexploration and state-action space coverage on the Pendulum task with state representation embedded into 1 dimension. The dots represent 500 state-action samples gathered using the latest policy (pessimistic (black) or optimistic (red)). Figure 9a displays the standard deviation (σ) of the two critics, with smaller values observed in well-explored state-action regions. In Figure 9b, we depict pessimistic policy probabilities. Due to lower bound optimization, the actor prioritizes state-action subspaces that have already been explored and do not yield critic disagreement. Figure 9c illustrates optimistic policy probabilities. Despite having similar entropy levels, following the upper bound policy results in better coverage within critic disagreement regions.

In the development of DAC, our aim was to enforce entropy and non-saturation within both the pessimistic and optimistic actors. DAC accomplishes this through distinct yet complementary methods for each actor. For the pessimistic actor, soft policy learning is employed to enforce entropy and prevent policy saturation. In contrast, the optimistic actor uses KL divergence as a means of maintaining similarity with the pessimistic actor and adhering to certain policy constraints. The incorporation of KL divergence in the optimistic actor's objective serves multiple purposes:

- 1. Reducing the degree of off-policy learning Given that exploration is conducted solely by the optimistic actor, the pessimistic actor updates entirely off-policy, using transitions sampled from the optimistic policy. This can potentially lead to unstable learning, a phenomenon known as the "deadly triad" (Sutton & Barto, 2018). Integrating KL divergence into the optimistic objective aligns the transitions sampled from the optimistic policy with the expectations under the pessimistic policy, thereby mitigating the extent of off-policy learning.
- 2. Anchoring the adjustment mechanisms As discussed in Section 4, the automatic adjustment of parameters β^o (optimism) and τ (KL penalty weight) depends on a target divergence value. Without the divergence penalty, these

adjustment mechanisms would have to be designed in a different way.

3. Preventing saturation of the optimistic policy - By minimizing the KL divergence between the optimistic and pessimistic actors, the optimistic actor is encouraged to emulate a policy trained via soft policy learning. This discourages the optimistic actor from policy saturation, maintaining the integrity of its actions.

In DAC, both the pessimistic and optimistic actors are represented as simple diagonal normal distributions, further transformed by the hyperbolic tangent (Tanh) activation. The KL divergence between these actors is computed in a closed form, utilizing the change of variables technique. Though this is a well-established result, we include it here for completeness. Denote x as samples from the policy distributions before the Tanh activation, p^p and p^o as the distributions of the pessimistic and optimistic actors on x, respectively. The application of Tanh is expressed as y = h(x), resulting in the transformed distributions π^p , π^o . Using the change of variables formula, the KL divergence is derived as follows:

$$KL(p_c|p_o) = \int_{-\infty}^{\infty} p^p(x) \log \frac{p^p(x)}{p^o(x)} dx$$

$$= \int_{-\infty}^{\infty} \pi^p(h(x)) \left| \frac{dy}{dx}(x) \right| \log \frac{\pi^p(h(x)) \left| \frac{dy}{dx}(x) \right|}{\pi^o(h(x)) \left| \frac{dy}{dx}(x) \right|} dx$$

$$= \int_{-\infty}^{\infty} \pi^p(y) \log \frac{\pi^p(y)}{\pi^o(y)} dy = KL(p^p|p^o)$$
(42)

This relationship holds for any distributions p_c and p_o . With the assumption of diagonal Gaussian distributions with dimensionality |A|, the KL divergence simplifies to:

$$KL(p_p|p_o) = KL(\pi_c|\pi_o) = \sum_{i=1}^{|A|} \left(\log \frac{\sigma_i^p}{\sigma_i^o} + \frac{(\sigma_i^o)^2 + (\mu_i^o - \mu_i^p)^2}{2(\sigma_i^p)^2} - \frac{1}{2} \right)$$
(43)

Using KL guarantees that the optimistic policy optimizes for a specified level of variance, which can be distinct from π_{ϕ}^p . To this end, we define the exploration variance multiplier m, which is a simple standard deviation multiplier. This leads to the following formulation of KL applied to DAC:

$$KL(\pi_c|\pi_o) = \sum_{i=1}^{|A|} \left(\log \frac{\sigma_i^p}{\bar{\sigma}_i^o} + \frac{(\bar{\sigma}_i^o)^2 + (\mu_i^o - \mu_i^p)^2}{2(\sigma_i^p)^2} - \frac{1}{2} \right), \quad \bar{\sigma}_i^o = \frac{\sigma_i^o}{m}$$
(44)

This approach ensures distinct entropy levels for TD learning and exploration while maintaining the standard convergence properties of Actor-Critic (AC) algorithms. In fact, if $\lim_{\mathcal{D}\to\infty}Q^{\sigma}_{\theta}(s,a)=0$ it follows that in the limit both actors recover a policy that differs only by m. While other differentiable divergence or distance functions could be used, the appeal of KL divergence lies in its closed-form solution for any invertible and differentiable transformation of the given distributions.

C.3. Adjustment of β^o and τ

Since values of Q^{μ}_{θ} and Q^{σ}_{θ} depend on reward scales, as well as aleatoric and epistemic uncertainty of the environment, the value of β^o cannot be easily set. DAC leverages an observation that for $\beta^o = -\beta^p$ the optimistic actor recovers the objective of the pessimistic actor. Then, β^o can be defined such that the divergence between the pessimistic baseline policy and the optimistic policy reaches a desired level, as shown in Equation 20. This adaptive approach, as illustrated in Figure 10, accommodates different scales of Q-values and contrasts with setups like OAC, where optimism is predefined by fixing β^o at a specific value. We find that the optimism and KL weight used by DAC are highly variable between tasks and even phase of the training, showing the advantage of the automatic adjustment mechanism as opposed to using predefined levels. Furthermore, we find that DAC generally uses much higher levels of optimism than values that were found optimal for OAC (Ciosek et al., 2019).

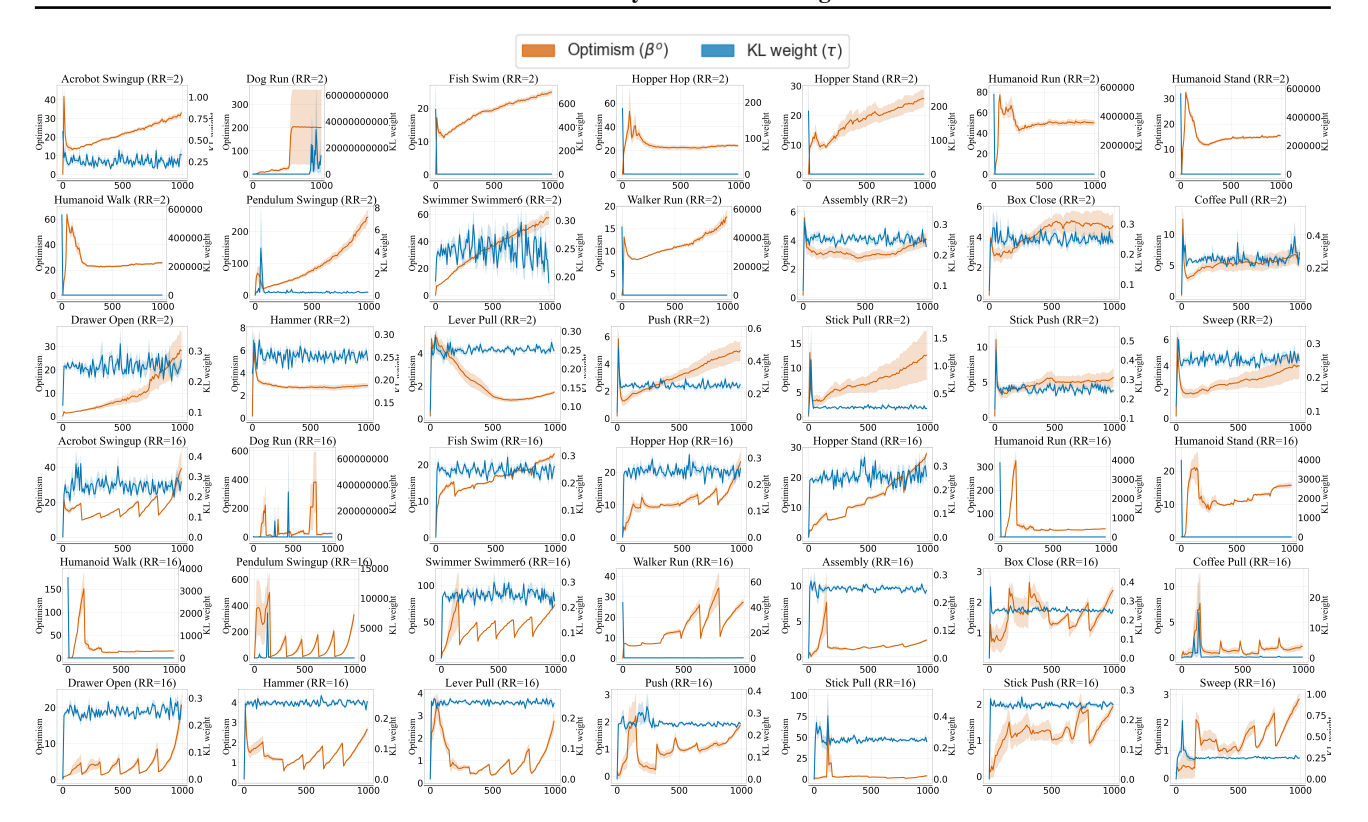


Figure 10. The observed levels of optimism (β^o) and KL weight (τ) during the training in both low and high replay regimes. As follows from the conducted measurements, the levels of optimism used by DAC depend not only upon the tested task, but also upon the phase of the training, with higher levels of optism seen in the latter training phases. Y-axis denotes the mean optimism (left axis) and KL weight (right axis) value with 3 standard deviation CI. 10 seeds per task.

C.4. Replay Ratio Scaling

Increasing the replay ratio was the key ingredient in increasing the sample efficiency and final performance of many recent RL agents (Janner et al., 2019; Chen et al., 2020; Hiraoka et al., 2021; Nikishin et al., 2022; Schwarzer et al., 2023). Moreover, many of the novelties brought by those agents were focused on stabilizing the learning given the high-replay regime (Janner et al., 2019; Chen et al., 2020; Hiraoka et al., 2021). A particularly interesting technique is scaling by resetting, as it is applicable to most off-policy RL algorithms. DAC improvements are largely orthogonal to the direction of increasing the replay ratio. Figures 1, 4 and 6 show DAC performance with and without scaling by resetting.

C.5. Non-soft value DAC derivation

In the main body of the paper, we derive and implement DAC as a pure MaxEnt algorithm, such that employs both soft policy and soft values. In this section, we discuss simpler derivations of the policy evaluation and improvement steps in DAC stemming from non-soft value functions. In such setup, value is defined as:

$$V^{\pi}(s) = \mathop{\mathbb{E}}_{a \sim \pi} r_{s,a} + V^{\pi}(s')$$
 (45)

Then, the optimistic actor can be defined as:

$$\begin{split} \pi_{\eta}^{o} &= \underset{\pi \in \Pi}{\arg \max} \; \mathbf{E} \; e^{\; 2\beta^{o} V_{\theta}^{i}(s) + \tau K L(\pi_{\eta}^{o}(s) | \pi_{\phi}^{p}(s))} \\ &\approx \underset{\pi \in \Pi}{\arg \max} \; \underset{s \sim \mathcal{D}}{\mathbf{E}} \; V_{\theta}^{\mu}(s) + \beta^{o} V_{\theta}^{\sigma}(s) - \tau K L(\pi_{\eta}^{o}(s) | \pi_{\phi}^{p}(s)) \\ &\approx \underset{\pi \in \Pi}{\arg \max} \; \underset{s \sim \mathcal{D}}{\mathbf{E}} \; Q_{\theta}^{\mu}(s, a) + \beta^{o} Q_{\theta}^{\sigma}(s, a) - \tau K L(\pi_{\eta}^{o}(s) | \pi_{\phi}^{p}(s)), \quad a \sim \pi_{\eta}^{o}(s) \end{split}$$
(46)

Given a non-soft value definition, the pessimistic actor can be defined as a "twin" of the optimistic one:

$$\pi_{\phi}^{p} = \underset{\pi \in \Pi}{\arg \max} \underset{s \sim \mathcal{D}}{\text{E}} e^{2\beta^{p} V_{\theta}^{i}(s) + \alpha K L(\pi_{\phi}^{p}|U)}$$

$$\tag{47}$$

Above, U denotes a uniform distribution with its domain over the entire action space. As such, whereas the optimistic actor minimizes the KL divergence to the pessimistic actor, and the pessimistic actor minimizes the KL divergence to a uniform distribution. Such definition retrieves entropy maximizing policy:

$$\pi_{\phi}^{p} \approx \underset{\pi \in \Pi}{\operatorname{arg \, max}} \underset{s \sim \mathcal{D}}{\overset{E}{\to}} V_{\theta}^{\mu}(s) + \beta^{p} V_{\theta}^{\sigma}(s) - KL(\pi_{\phi}^{p}(s)|U(s))$$

$$= \underset{\pi \in \Pi}{\operatorname{arg \, max}} \underset{s \sim \mathcal{D}}{\overset{E}{\to}} V_{\theta}^{\mu}(s) + \beta^{p} V_{\theta}^{\sigma}(s) + \alpha \mathcal{H}(s)$$

$$\approx \underset{\pi \in \Pi}{\operatorname{arg \, max}} \underset{s \sim \mathcal{D}}{\overset{E}{\to}} Q_{\theta}^{\mu}(s, a) + \beta^{p} Q_{\theta}^{\sigma}(s, a) - \alpha \log \pi_{\phi}^{p}(a|s), \quad a \sim \pi_{\phi}^{p}(s)$$

$$(48)$$

D. Additional Experiments

D.1. Simplified and Regular DAC

In our investigation, we assess the effectiveness of the regular Dual Actor-Critic (DAC) architecture, where the optimistic policy is a perturbation of the pessimistic one, against a simplified architecture that treats the optimistic policy as independent. The primary focus is on performance disparities across all 21 tasks listed in Table 2, considering both low and high replay ratios. These findings are illustrated in Figure 11.

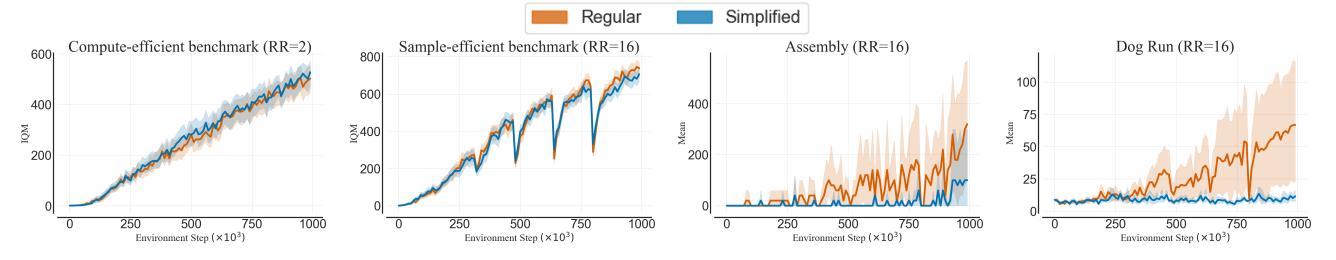


Figure 11. We compare the performance of the simplified and regular DAC architectures. We find that the simplified architecture yields very similar performance, except for the more complex tasks where the regular architecture dominates. 21 tasks and 10 seeds per task.

We find that the simplified DAC architecture generally performs on par with the regular one. However, the regular architecture demonstrates superior performance in more challenging domains, particularly dog and assembly tasks. This suggests that the regular DAC approach of defining the optimistic policy as perturbation offers advantages in complex environments. The two architectures differ in their approaches to controlling the KL divergence between the optimistic and pessimistic actors. In the regular DAC setup, the optimistic policy, being a perturbation of the pessimistic policy, can reduce its output to achieve a desired divergence level, independently of the pessimistic policy location. Conversely, in the simplified architecture, the independent optimistic actor must continually adapt to align with the pessimistic policy across the state-action space - posing a challenge in maintaining a stable divergence. To this end, we find that the simplified DAC architecture is not able to meet the target divergence on the dog and assembly task.

D.2. Layer Normalization

Recently, there has been a surge of works exploring the importance of critic regularization in high replay regimes (Liu et al., 2020; Laskin et al., 2020; Hiraoka et al., 2021; Gogianu et al., 2021; Li et al., 2022; D'Oro et al., 2022). Whereas there is still a lot to understand about the interplay of TD learning and network regularization, it is clear that a regularized critic allows a higher replay ratio to be used (Hiraoka et al., 2021; Li et al., 2022; D'Oro et al., 2022). In this paper, we explore only one method that could be considered regularization, that is full-parameter resets (Nikishin et al., 2022; D'Oro et al., 2022). Given the effectiveness of the only regularization we tested, we hypothesize that experimenting with methods like layer normalization (Ba et al., 2016), weight decay (Krogh & Hertz, 1991), spectral normalization (Gogianu et al., 2021) or dropout (Srivastava et al., 2014) could further improve DAC performance. We investigate the effects of layer normalization on DAC performance in Figure 12 and leave further regularization studies for future work.

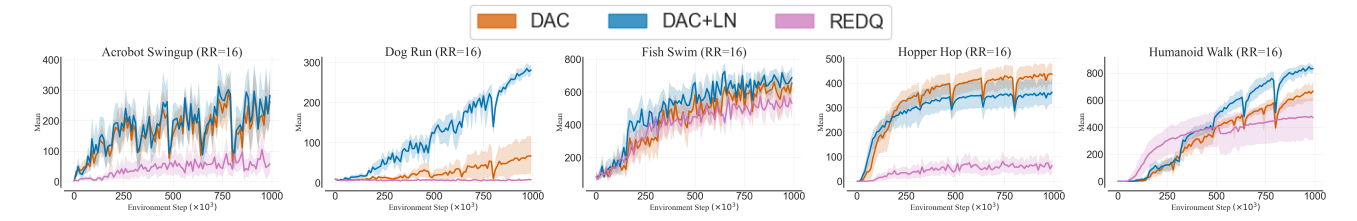


Figure 12. We investigate the effects of layer normalization on DAC critic and find that it significantly improves performance on the considered locomotion tasks. 10 seeds per task.

We find that using layer normalization on critic within the DAC design significantly improves its performance on locomotion tasks. This results is in line with previous work that augmented other RL algorithms with layer normalization (Li et al., 2022; Hiraoka et al., 2021; Lyle et al., 2023; Ball et al., 2023; Cetin & Celiktutan, 2023)

D.3. Critic Overestimation

Here, we investigate whether the decoupled architecture (using a conservative policy for TD updates and optimistic policy for exploration) indeed mitigates Q-value overestimation characteristic for non-conservative updates (Fujimoto et al., 2018; Kuznetsov et al., 2020; Moskovitz et al., 2021; Cetin & Celiktutan, 2023). As such, we compare the environment returns to the returns implied by the critic, according to the following:

$$O_{\theta} = \frac{Q_{\theta}(s, a)}{Q^{\pi}(s, a)} \tag{49}$$

Where O_{θ} denotes the overestimation metric, $Q_{\theta}(s,a)$ is the critic output and $Q^{\pi}(s,a)$ stands for the observed empirical returns. Whereas the metric does not perfectly measure the overestimation, it allows to investigate the relative overestimation in the group of considered algorithms. As shown in Figure 13, we find that the dual architecture prevents the overestimation associated with optimistic TD updates and yields measurements similar to other risk-aware algorithms.

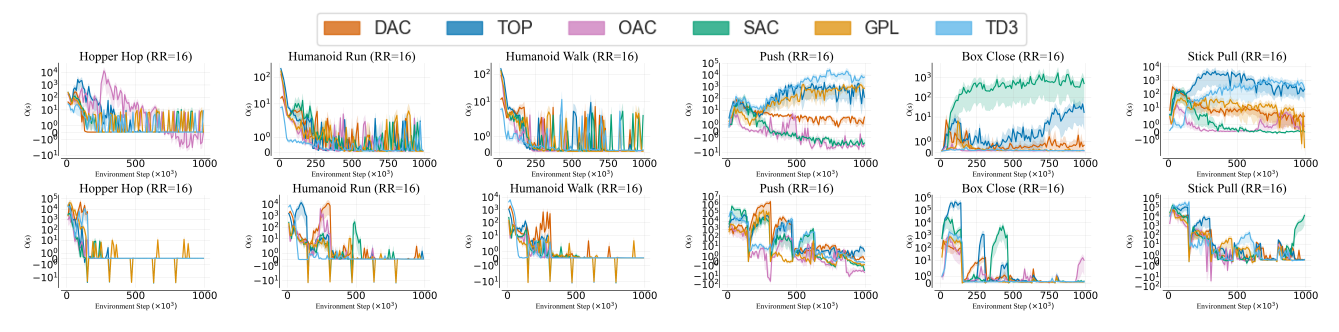


Figure 13. We investigate if the dual architecture allows to mitigate the value overestimation associated with optimistic algorithms. Indeed, the measured overestimation (shown on the Y-axis) is similar across all tested algorithms. 10 seeds per task.

E. Experimental Details

E.1. Low and High Replay Regimes

We consider two replay regimes:

- Compute-Efficient Regime each algorithm performs 2 gradient update loops per environment step.
- Sample-Efficient Regime each algorithm performs 16 gradient update loops per environment step, with full-parameter resets every 160k environment steps. This configuration is based on the one described in (D'Oro et al., 2022).

The evaluation spans 1mln environment steps on 21 tasks listed in Table 2. The set of tested algorithms includes:

- DAC Dual Actor-Critic. The approach proposed in this paper, described in detail in Section 4 and Appendix C.
- SAC Soft Actor-Critic (Haarnoja et al., 2018) builds on DDPG (Silver et al., 2014). SAC extends the DDPG algorithm with features such as a stochastic policy using the reparametrization trick, automatic entropy temperature adjustment, Clipped Double Q-learning, and maximum entropy updates for actor and critic networks.
- TD3 Twin Deep Deterministic Policy Gradient (Fujimoto et al., 2018) is an extension of the DDPG algorithm, including a target actor network and Clipped Double Q-learning.
- OAC Optimistic Actor-Critic (Ciosek et al., 2019) extends SAC with an optimistic exploration policy approximating the Q-value upper bound.
- TOP Tactical Optimism and Pessimism (Moskovitz et al., 2021) addresses the optimism-pessimism dilemma with an external discrete bandit learning β^p from predefined values. Initially based on TD3, the implementation here uses SAC due to its better performance.
- GPL Generalized Pessimism Learning (Cetin & Celiktutan, 2023) proposes updating pessimism in the pessimistic value approximation V_{β}^{π} through a dual optimization objective.

We standardize the common hyperparameters between all algorithms to minimize the differences between all implementations. We align the basic values with the state-of-the-art SAC implementation (D'Oro et al., 2022). We employ uniform network architectures and a standard ensemble of two critics (Fujimoto et al., 2018; Haarnoja et al., 2018; Ciosek et al., 2019; Moskovitz et al., 2021; Cetin & Celiktutan, 2023). We report the detailed hyperparameter values in Appendix F. The results for these experiments are presented in Figures 1, 4, 6 and 14.

Table 2. 21 tasks used for the evaluation of model-free algorithms in low and high replay ration regimes.

LOW AND HIGH REPLAY RATIO		
DEEPMIND CONTROL	METAWORLD	
ACROBOT (SWINGUP)	ASSEMBLY	
Dog (Run)	Box (Close)	
FISH (SWIM)	Coffee (Pull)	
Hopper (Hop, Stand)	Drawer (Open)	
HUMANOID (RUN, STAND, WALK)	HAMMER	
PENDULUM (SWINGUP)	Lever (Pull)	
SWIMMER (SWIMMER6)	Push	
Walker (Run)	STICK (PULL, PUSH)	
	SWEEP	

E.2. Comparison Against Model-Based

We evaluate the following set of continuous-action model-based and model-free algorithms:

- DreamerV3 a state-of-the-art model-based algorithm (Hafner et al., 2023). It was shown to perform well across a wide range of tasks, including DMC.
- TD-MPC Temporal Difference Learning for Model Predictive Control (Hansen et al., 2022) a state-of-the-art model-based algorithm leveraging model of the environment for critic-bootstrapped model-predictive control.
- D4PG Distributed Distributional Deterministic Policy Gradients (Barth-Maron et al., 2018) is a distributed version of DDPG leveraging distributional critics, prioritized experience buffer and N-step returns.
- MPO Maximum a Posteriori Policy Optimisation (Abdolmaleki et al., 2018) is an off-policy algorithm based on coordinate ascent on a relative entropy objective.

For those algorithms, we source the original results reported by the authors of the respective method. In this setup, we consider two sets of environments:

- Easy to medium tasks this set includes tasks chosen based on a common intersection of all results reported at 500k environment steps by the algorithms under consideration.
- Complex tasks This set comprises 5 of the most challenging tasks from the DMC suite, known to be solvable by pure RL algorithms. For these complex tasks, the comparison is specifically against TD-MPC, as it was shown to reliably solve dog tasks with proprioceptive input, as per (Hansen et al., 2022). To better evaluate performance, a prolonged training duration of 3mln environment steps is implemented, with an action repeat of 2, consistent with the original TD-MPC setup. Additionally, to minimize the architecture complexity gap between DAC and TD-MPC, DAC employs the TD-MPC critic architecture, including an extra hidden layer and the use of layer normalization.

All tasks included in these experiments are detailed in Table 3. The results of these experiments are showcased in Figures 5, 15 and 16.

Comparison Against Model-Based			
10 Easy to Medium (500k steps)	5 COMPLEX (3MLN STEPS)		
ACROBOT (SWINGUP)	Dog (Run, Trot, Walk)		
CARTPOLE (SWINGUP-SPARSE)	Humanoid (Run, Walk)		
CHEETAH (RUN)			
FINGER (SPIN, TURN-HARD)			
HOPPER (HOP)			
Reacher (Easy, Hard)			
Walker (Run, Walk)			

Table 3. 15 tasks used for the evaluation of DAC against model-based algorithms.

E.3. Hyperparameter Sensitivity & Design Choices

In the experiments addressing hyperparameter sensitivity and design choices, we evaluate the configurations on a selected set of 15 tasks, as outlined in Table 4. These tasks represent a subset of the 21 tasks used in the main experiment. Each configuration is executed for a duration of 500k environment steps.

E.3.1. Hyperparameter Sensitivity

In our study on the hyperparameter sensitivity of the proposed approach, we focus on several key hyperparameters, examining their impact on the performance of the algorithm. We list the introduced hyperparameters along with the tested values below, with the results for this evaluation is presented in Figure 7.

- KL divergence target (\mathcal{KL}^*) this parameter represents the desired KL divergence between the pessimistic and optimistic policies. When the observed KL divergence exceeds this target, DAC adjusts by decreasing β^o (reducing the risk appetite of the optimistic actor) and increasing τ (enhancing the influence of KL regularization). The KL target is defined per action dimension, as detailed in Equation 20. The values tested for \mathcal{KL}^* are: 0.05, 0.25, 0.5, and 0.75.
- Standard deviation multiplier (m) this hyperparameter determines the ratio between the standard deviations of the optimistic and pessimistic policies. For instance, if m=2, the standard deviation targeted by the optimistic policy will be double that of the pessimistic policy, as defined in Equation 44. The considered values for m are: 0.75, 1.0, 1.25, and 1.5.
- Adjustment mechanism optimizer settings the adjustment mechanism for β^o and τ is gradient-based and thus requires specific optimizer settings, including the learning rate. The same optimizer settings are applied to both β^o and τ . The learning rates evaluated are: 3e-5, 3e-4, 3e-3, and 3e-2.

E.3.2. DESIGN CHOICES

In this section, we explore various simplifications of DAC design to assess their impact on performance. These modifications involve alterations to the structure and behavior of the actors in the DAC framework. The specific design simplifications considered are:

- Single policy π_{η}^{o} this variant employs SAC with only an optimistic actor, thus relying solely on the optimistic policy for exploration, TD learning, and evaluation. Due to the presence of a single actor, the optimism adjustment mechanism is not applicable in this setup.
- Deterministic π^p_ϕ DAC is modified to have a completely deterministic pessimistic actor, while the optimistic actor remains stochastic and responsible for exploration. This setup often leads to an overestimation of Q-values, indicating the potential regularizing effect of soft SARSA.
- Deterministic π^o_η in this configuration, the optimistic actor of DAC is made fully deterministic. Consequently, the exploration policy becomes deterministic and greedily maximizes the Q-value upper bound.
- DAC simplified this refers to the streamlined version of DAC, as described in Section 4.
- No KL regularization this DAC variant removes the KL penalty on the optimistic actor, allowing it to diverge from the conservative actor without constraints.
- No τ and β^o adjustment this variant operates without automatic adjustments to the rate of optimism and the KL weight, keeping these parameters fixed throughout training.
- No β^o adjustment DAC is modified to retain the automatic adjustment of the KL weight, but without the automatic adjustment of optimism.
- No τ adjustment DAC without the automatic adjustment of the KL weight, albeit still using the automatic adjustment of the optimism.

The findings from the DAC design simplifications, as detailed in Table 1, reveal some intriguing insights into the dynamics of actor behavior within the DAC framework. Firstly, the variant with a deterministic pessimistic actor exhibits relatively poor performance. Interestingly, it underperforms compared to the configuration with a deterministic optimistic actor, which employs deterministic greedy exploration. This outcome suggests that incorporating variance in TD learning may offer benefits that warrant further investigation. The deterministic pessimistic actor's subpar performance indicates the potential significance of stochastic elements in policy learning. Furthermore, in low replay settings, the simplified DAC design performs comparably to the regular DAC model. However, a notable performance gap emerges in high replay scenarios. This finding indicates that the regular architecture may be more beneficial when the learning is more aggressive. Finally, the results demonstrate a synergistic effect when both β^o (optimism rate) and τ (KL weight) are subject to adjustment mechanisms. This synergy leads to performance improvements that surpass those achieved by adjusting either parameter individually. This suggests that the interplay between optimism in policy and KL regularization is crucial for balancing exploration and exploitation, and for achieving optimal performance. These insights highlight the importance of carefully considering the balance between deterministic and stochastic elements in actor designs.

Table 4. 15 tasks used for the evaluation of DAC hyperparameter sensitivity and design choice evaluation.

Hyperparameter Sensitivity & Design Choices			
DEEPMIND CONTROL	METAWORLD		
ACROBOT (SWINGUP)	Box (Close)		
FISH (SWIM)	DRAWER (OPEN)		
HOPPER (HOP, STAND)	Hammer		
HUMANOID (RUN, STAND, WALK)	Push		
PENDULUM (SWINGUP)	SWEEP		
SWIMMER (SWIMMER6)			
Walker (Run)			

F. Learning Curves and Hyperparameters

Table 5. We take hyperparameter values proposed by the authors of the respective method.

Метнор	Hyperparameter	VALUE
	NETWORK SIZE	(256, 256)
	ACTIVATIONS	RELU
	CRITIC ENSEMBLE SIZE	2
	ACTION REPEAT	1
	Optimizer	ADAM
SAC / SHARED	LEARNING RATE	3e-4
	BATCH SIZE	256
	DISCOUNT	0.99
	Initial Temperature	1.0
	INITIAL STEPS	10000
	TARGET ENTROPY	$ \mathcal{A} /2$
	Polyak Weight	0.005
	POLICY UPDATE DELAY	2
TD3	Exploration σ	0.5
1D3	Target Policy σ	0.2
	EXPLORATION NOISE CLIP	± 0.5
	OPTIMISM	4.36
OAC	PESSIMISM	-1.0
	KL DIVERGENCE CONSTRAINT	3.69
ТОР	OPTIMISTIC ARM	0.0
	PESSIMISTIC ARM	-1.0
101	Bandit Learning Rate	0.1
	BANDIT DECAY	0.9
GPL	INITIAL P PESSIMISM	-0.5
GFL	PESSIMISTIC LEARNING RATE	1e-4
	PESSIMISM	-0.33
	Initial Optimism	0.5
DAC	Initial KL Weight	0.25
DAC	TARGET KL DIVERGENCE	0.25
	STANDARD DEVIATION MULTIPLIER	1.25
	ADJUSTMENT LEARNING RATE	3e-5

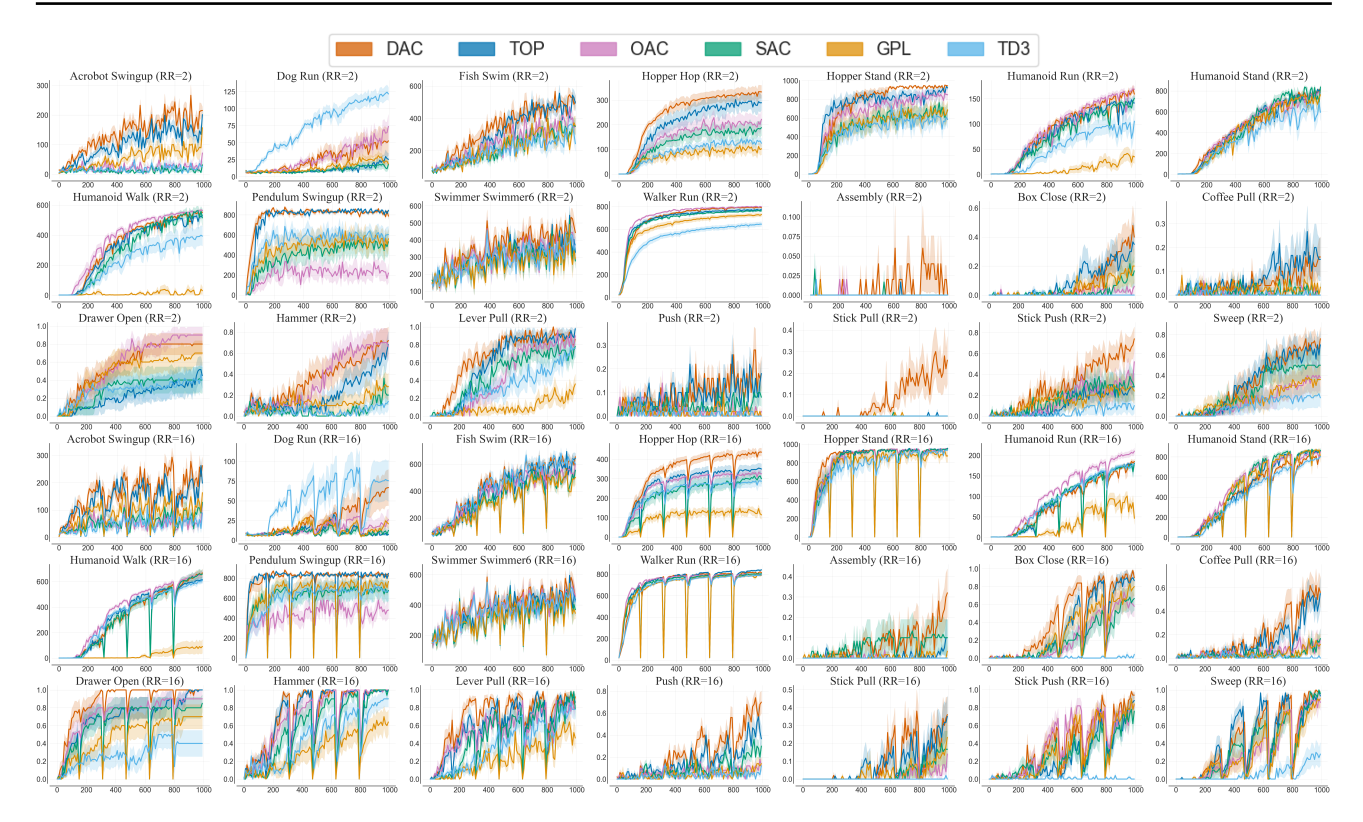


Figure 14. Learning curves for the compute-efficient (2 gradient steps per environment step) and sample-efficient (16 gradient steps per environment step and full-parameter resets every 160k environment steps) benchmarks. Y-axis reports mean with 3 standard deviations. 10 seeds per task.

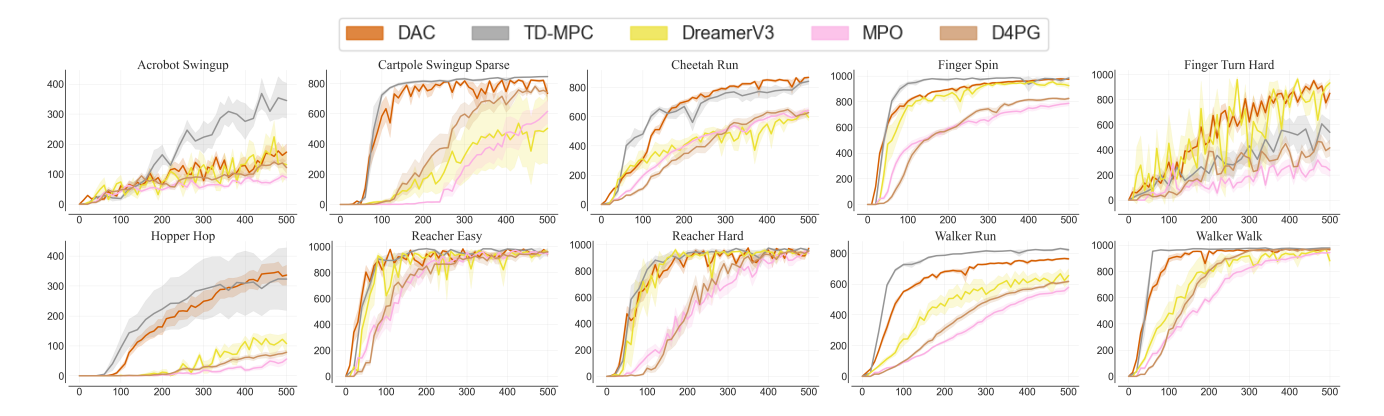


Figure 15. Learning curves for the easy to medium tasks taken from the DreamerV3 and TD-MPC evaluations. X-axis denotes the environment steps in thousands; and Y-axis reports mean with 3 standard deviations. 10 seeds per task.

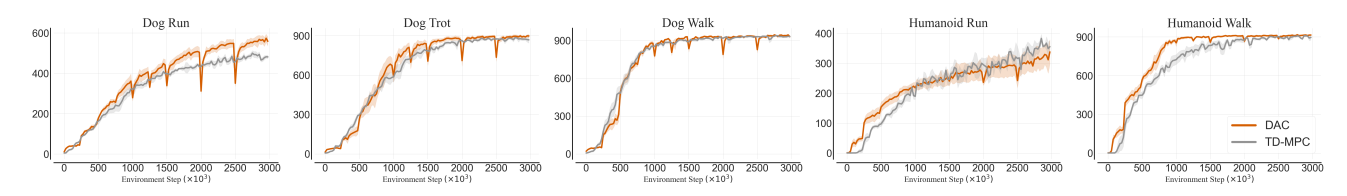


Figure 16. Learning curves for the complex tasks taken TD-MPC evaluations. To assure the consistency of results we use action repeat of 2 (ie. the value used by TD-MPC). X-axis denotes the environment steps in thousands; and Y-axis reports mean with 3 standard deviations. 5 seeds per task.